Environmental Pollution 271 (2021) 116358

Contents lists available at ScienceDirect

Environmental Pollution

journal homepage: www.elsevier.com/locate/envpol

Tracking gene expression, metabolic profiles, and biochemical analysis in the halotolerant basidiomycetous yeast *Rhodotorula mucilaginosa* EXF-1630 during benzo[a]pyrene and phenanthrene biodegradation under hypersaline conditions☆

Liliana Martínez-Ávila [a], Heidy Peidro-Guzmán [a], Yordanis Pérez-Llano [a], Tonatiuh Moreno-Perlín [a], Ayixon Sánchez-Reyes [b], Elisabet Aranda [c], Gabriela Ángeles de Paz [c], Arline Fernández-Silva [d], Jorge Luis Folch-Mallol [e], Hubert Cabana [f], Nina Gunde-Cimerman [g], Ramón Alberto Batista-García [a, *]

[a] *Centro de Investigación en Dinámica Celular, Instituto de Investigación en Ciencias Básicas y Aplicadas, Universidad Autónoma del Estado de Morelos, Cuernavaca, Morelos, Mexico*
[b] *Cátedras Conacyt – Instituto de Biotecnología. Universidad Nacional Autónoma de México, Cuernavaca, Morelos, Mexico*
[c] *Instituto Universitario de Investigación del Agua, Universidad de Granada, Granada, Spain*
[d] *Centro de Investigaciones Químicas, Instituto de Investigación en Ciencias Básicas y Aplicadas, Universidad Autónoma del Estado de Morelos, Cuernavaca, Morelos, Mexico*
[e] *Centro de Investigación en Biotecnología, Universidad Autónoma del Estado de Morelos, Cuernavaca, Morelos, Mexico*
[f] *Faculté de Genié, Université de Sherbrooke, Sherbrooke, Quebec, Canada*
[g] *Departament of Biology, Biotechnical Faculty, University of Ljubljana, Ljubljana, Slovenia*

A R T I C L E I N F O

Article history:
Received 9 September 2020
Received in revised form
16 December 2020
Accepted 17 December 2020
Available online 18 December 2020

Keywords:
Polycyclic aromatic hydrocarbons
Transcriptomic
PAH metabolites
Bioremediation
Halotolerant yeasts
Benzo[a]pyrene
Phenanthrene
Rhodotorula mucilaginosa

A B S T R A C T

Polyaromatic phenanthrene (Phe) and benzo[a]pyrene (BaP) are highly toxic, mutagenic, and carcinogenic contaminants widely dispersed in nature, including saline environments. Polyextremotolerant *Rhodotorula mucilaginosa* EXF-1630, isolated from Arctic sea ice, was grown on a huge concentration range -10 to 500 ppm- of Phe and BaP as sole carbon sources at hypersaline conditions (1 M NaCl). Selected polycyclic aromatic hydrocarbons (PAHs) supported growth as well as glucose, even at high PAH concentrations. Initially, up to 40% of Phe and BaP were adsorbed, followed by biodegradation, resulting in 80% removal in 10 days. While extracellular laccase, peroxidase, and un-specific peroxygenase activities were not detected, NADPH-cytochrome *c* reductase activity peaked at 4 days. The successful removal of PAHs and the absence of toxic metabolites were confirmed by toxicological tests on moss *Physcomitrium patens,* bacterium *Aliivibrio fischeri*, human erythrocytes, and pulmonary epithelial cells (A549). Metabolic profiles were determined at the midpoint of the biodegradation exponential phase, with added Phe and BaP (100 ppm) and 1 M NaCl. Different hydroxylated products were found in the culture medium, while the conjugative metabolite 1-phenanthryl-β-D-glucopyranose was detected in the medium and in the cells. Transcriptome analysis resulted in 870 upregulated and 2,288 downregulated transcripts on PAHs, in comparison to glucose. Genomic mining of 61 available yeast genomes showed a widespread distribution of 31 xenobiotic degradation pathways in different yeast lineages. Two distributions with similar metabolic capacities included black yeasts and mainly members of the Sporidiobolaceae family (including EXF-1630), respectively. This is the first work describing a metabolic profile and transcriptomic analysis of PAH degradation by yeast.

☆ This paper has been recommended for acceptance by Christian Sonne.

* Corresponding author. Centro de Investigación en Dinámica Celular, Instituto de Investigación en Ciencias Básicas y Aplicadas, Universidad Autónoma del Estado de Morelos, Ave. Universidad 1001. Col. Chamilpa, Cuernavaca, Morelos, CP 62209, Mexico.
E-mail addresses: rabg@uaem.mx, rbatista25@yahoo.com (R.A. Batista-García).

https://doi.org/10.1016/j.envpol.2020.116358
0269-7491/

1. Introduction

Bioremediation is an eco-friendly, efficient, and safe technology for the restoration of polluted ecosystems. It is based on the microbial ability to transform xenobiotics (e.g. polycyclic aromatic hydrocarbons -PAHs-) into less toxic compounds (Srivastava and Kumar, 2019). Fungi are well established microbial agents for bioremediation due to their capability to degrade different environmentally recalcitrant compounds (e.g. benzo[a]pyrene -BaP- and phenanthrene -Phe-) (Prenafeta-Boldú et al., 2019; Srivastava and Kumar, 2019; Dacco et al., 2020). While filamentous fungi have been extensively studied as PAHs-bioremediating agents, yeasts emerged later as aromatic compound-utilizing microorganisms (Garapati and Mishra, 2012; Hashem et al., 2018; Yaguchi et al., 2020). In particular, different yeast species belonging to the genera *Aureobasidium, Candida, Exophiala, Pichia, Rhodosporidium, Rhodotorula, Trichosporon* (now *Cutaneotrichosporon*), and *Yarrowia* have been recognized for their ability to remove pollutants (e.g. PAHs, phenolic compounds, radioactive wastewaters) (Jarboui et al., 2012; Margesin, 2014; Hashem et al., 2018; Tkavc et al., 2018; Shuryak et al., 2019; Belloch et al., 2020; Yaguchi et al., 2020).

PAH biodegradation rates are influenced by different environmental conditions (Gupta et al., 2015; Guarino et al., 2017; Alegbeleye et al., 2017). Many PAHs-polluted ecosystems (e.g. estuaries, hypersaline brines, oil-based drilling muds, marine environments) are saline due to different concentrations of NaCl and/or other salts (McGenity, 2016). Low water activity stress under these conditions restricts microbial diversity and growth, decreases oxygen solubility, and affects chemical properties of organic xenobiotics, resulting in hindered hydrocarbon biodegradation. Halotolerant fungi (including yeasts) thus represent promising candidates for the implementation of bioremediation strategies in hypersaline conditions, or even at (poly)extreme conditions (Jiang et al., 2015; Bano et al., 2018; Kamyabi et al., 2018; Ali et al., 2019; González-Abradelo et al., 2019). There is scarce information on metabolic and genome-scale transcriptomic responses of yeast to deplete and detoxify organic xenobiotics, and in particular, (poly) aromatic compounds (Blasi et al., 2017; Kamyabi et al., 2018; Kashyap et al., 2020).

In this study, we used transcriptomic, metabolic profiling, and different biochemical and toxicological tests to analyze the mechanisms underlying PAH biodepletion by the polyextremotolerant basidiomycetous yeast *Rhodotorula mucilaginosa* EXF-1630 when grown at hypersaline conditions (1 M NaCl) with Phe and BaP as sole carbon sources. Phe and BaP are widespread polyaromatic contaminants in nature, with high toxicity, mutagenicity, and carcinogenicity (Haritash and Kaushik, 2009). To the best of our knowledge, no previous work has been published describing a metabolic profile and transcriptomic analysis of PAH degradation by yeast and still less under hypersaline conditions.

2. Materials and methods

2.1. Yeast strain and molecular identification

Rhodotorula mucilaginosa EXF-1630 used in this study was isolated in 2001 from sea ice in Arctic Kongsfjorden, Svalbard (Norway). The yeast strain was grown and maintained on Yeast-Nitrogen Base (YNB, Qbiogene) with 0.5% ammonium sulfate and 2% glucose (YNG medium). It was preserved in 20% glycerol at −80 °C in the Ex Microbial Culture Collection of the Infrastructural Centre Mycosmo, Department of Biology, Biotechnical Faculty, University of Ljubljana (Slovenia). For molecular taxonomical identification 24 highly conserved protein markers (alaS, cgtA, coaE, gmk, pgk, rplB, rplC, rplD, rplE, rplF, rplI, rplP, rplO, rplQ, rplW, rpmA, rpmL, rpsB, rpsI, rpsK, rpsL, rpsM, rpsP, tsf (Ren et al., 2016)) were extracted from the strain transcriptome and from other 27 genomes of the Sporidiobolaceae family. The sequences were concatenated and aligned with MAFFT software version 7.310 with default settings (Katoh et al., 2013). Gblocks version 0.91b was used to eliminate poorly aligned regions from the multiple sequence alignment (Castresana, 2000). Phylogenetic reconstruction was inferred from the multiple sequence alignment under a generalized time-reversible model using FastTree software version 2.1.10 under the maximum-likelihood approach (Price et al., 2010). Other options were set as default. Figtree version 1.4.3 (http://tree.bio.ed.ac.uk/software/figtree/) was used to display the summarized and annotated tree produced by the reconstruction steep.

2.2. NaCl tolerance and polycyclic aromatic hydrocarbon utilization by Rhodotorula mucilaginosa EXF-1630

A two-day-old pre-culture of *R. mucilaginosa* EXF-1630 incubated at 28 °C and 150 rpm was obtained in 10 mL of YNG medium. Cells were recovered by centrifugation at 10,000×*g* for 10 min at 4 °C and resuspended in saline solution (0.85%). Ten microliters of cell solution ($OD_{600\ nm} = 0.2$) were used as inoculum for the halotolerance experiments. Halotolerance of *R. mucilaginosa* EXF-1630 was determined on YNG agar medium supplemented with different NaCl concentrations: 0, 0.5, 1, 1.5, 2, 3, 4, and 5 M. Cultures were incubated at 15 °C and 28 °C.

For the primary screening of PAH utilization, cells were inoculated as described above on hypersaline (1 M NaCl) solid minimal medium supplemented with 1,8 diaminonaphthalene (Sigma-Aldrich, Saint Louis, U.S., Catalogue D21405), fluorene (Sigma-Aldrich, Saint Louis, U.S., Catalogue 128333), anthracene (Sigma-Aldrich, Saint Louis, U.S., Catalogue A89200), Phe (Sigma-Aldrich, Saint Louis, U.S., Catalogue P11409), pyrene (Sigma-Aldrich, Saint Louis, U.S., Catalogue, 185515), BaP (Sigma-Aldrich, Saint Louis, U.S., Catalogue B1760), or a mixture of Phe and BaP (1:1). Different final hydrocarbon concentrations were used (10, 20, 40, 60, 80, 100, 200, and 500 ppm) as sole carbon source. The composition of the used minimal medium can be found in González-Abradelo et al. (2019). A culture on 2% glucose was included as a control. Cultures were incubated at 28 °C for 10 days and a photographic record of the colonies was taken daily. From these experiments, PAHs and salt concentration were selected to proceed with the next analyses (see below).

The growth kinetics for the selected PAHs were determined in hypersaline (1 M NaCl) liquid minimal medium supplemented with 2% glucose, Phe, BaP, or a mixture of Phe and BaP (1:1) as sole carbon sources. PAHs were used at 100 ppm final concentration. Five hundred milliliter flasks containing 150 mL of minimal medium were inoculated to a starting $OD_{600\ nm}$ of 0.2. Absorbance at 600 nm was measured daily for 10 days using a Biotek® Epoch™ microplate spectrophotometer. Biomass productivity and growth rate were determined. All experiments were made in triplicates ($n = 3$).

2.3. Phenotype characterization of Rhodotorula mucilaginosa EXF-1630 during polyaromatic hydrocarbon exposure

Yeast cells exposed to Phe, BaP, a mixture of Phe and BaP (1:1, 100 ppm final concentration), and 2% glucose in hypersaline liquid medium were microscopically observed on a Zeiss Axio Observer microscope with a 100 × DIC objective (Carl Zeiss Microscopy, 440782-9902-000) (Zeiss Corp., Thornwood, New York, U.S.). The images were captured with an AxioCamMR3 camera (Zeiss Corp., Thornwood, New York, U.S.) connected to the microscope and exported using the ZEN 2012 (blue edition) software version 1.1.1.0.

Images from 25 microscopic fields were taken to quantify the number of cells, the number of budding cells per microliter, and cell size expressed in cm^2. ImageJ 1.52p (Wayne Rasband National Institute of Health, U.S.; http://rsb.info.nih.gov/ij/) was used to analyze the images quantitatively.

Changes in the hydrodynamic radius and Z-potential of three-day-old cultures of *R. mucilaginosa* EXF-1630 in the presence of Phe and BaP at hypersaline conditions were measured by dynamic light scattering (DLS). Measurements were performed on a Malvern Zetasizer Nano ZSP Spectrophotometer (Malvern Panalytical, Taren Point, Australia) with a scattering angle of 173°. Three runs with 10 scans of 10 s each were obtained for each measured data point, and then three sequential points were used to calculate the variation in the measurements. The data were used to obtain translational diffusion coefficients through the measurement of the correlation coefficient. Hydrodynamic radius was obtained from the translational diffusion coefficient, via the Stokes-Einstein equation. Results were analyzed using the Malvern software Zetasizer Nano DTS version 5.10.

2.4. Biochemical characterization of the biodegradation of phenanthrene and benzo[a]pyrene under hypersaline conditions by Rhodotorula mucilaginosa EXF-1630

Yeast cells of a two-day-old pre-culture of *R. mucilaginosa* EXF-1630 were collected as described above and washed three times with saline solution (0.85%), then incubated at 28 °C and 150 rpm for 18 h to deplete nutrients accumulated during the yeast growth in YNG medium. Cells were recovered by centrifugation as previously described. Liquid cultures in 250 mL flasks containing 50 mL of minimal medium, 1 M NaCl, and a mixture of Phe and BaP (1:1, 100 ppm as final concentration) were inoculated to a starting $OD_{600\ nm}$ of 0.2. Cultures were incubated at 28 °C and 150 rpm for 10 days.

Total removal, bioadsorption, and biodegradation of Phe and BaP were quantified at 2, 4, 6, 8, and 10 days of PAHs exposure using a gas chromatograph coupled to a mass spectrometer (GC-MS). The analytical procedure is described in González-Abradelo et al. (2019). Briefly, solvent extractions using 2 mL of mass-spectrometry (MS) grade hexane from supernatants and cells were performed after yeast growth with PAHs (Aranda et al., 2010). Abiotic controls with and without PAHs were implemented. Bioadsorption, biodegradation, and total removal were determined as described in González-Abradelo et al. (2019).

The pH was determined at each sampling point. Also, changes in the chemical oxygen demand (COD) were measured using *Accu*SPEC COD Digestion Tubes kit (SCP Science, California, U.S., Catalogue 250-130-026) according to manufacturer instructions. Enzymatic tests were conducted to determine laccase, peroxidase, and un-specific peroxygenase activities in the supernatants of yeast treatments (Camacho-Morales et al., 2018; González-Abradelo et al., 2019). NADPH-cytochrome *c* reductase activity was quantified using an NADPH assay kit (Sigma-Aldrich, Saint Louis, U.S., Catalogue CY0100). One international unit (IU) of enzymatic activity was defined as the amount of enzyme per milligram of protein catalyzing the oxidation of 1 mmol of substrate per minute.

Three independent experiments were made with three technical replicates each one (n = 9). All experimental determinations were also performed in triplicate for each sample.

2.5. Toxicological evaluation after polycyclic aromatic hydrocarbon removal by Rhodotorula mucilaginosa EXF-1630

Residual concentrations of Phe and BaP after 10-days yeast treatment, as well as possible toxic intermediate metabolites, were extracted with hexane and ethyl acetate from 10 mL of treated supernatants (Aranda et al., 2010). Three consecutive extractions were performed for each case. Two milliliters concentrated fractions were prepared after solvent evaporation at 40 °C, and metabolites were resuspended in 1 mL of methanol. Extracts from non-inoculated flasks with or without PAHs (controls) were also included in the toxicological tests. Toxicity was determined on four different systems: the moss *Physcomitrium patens* (named before as *Physcomitrella patens*), the luminescent bacterium *Aliivibrio fischeri*, whole blood human cells, and the cell line A549 (pulmonary epithelial cells).

Assays on *P. patens* were performed as described in Peidro-Guzmán et al. (2020). Briefly, fresh colonies of *P. patens* were incubated for 44 days in the presence of the enriched fractions obtained from the culture after yeast growth with PAHs. The relative growth rate of *P. patens* was determined from a photographic record of the moss colonies (Medina-Andrés et al., 2015). Toxicological assays using pure solvents (hexane and methanol) were implemented as controls. Nine moss explants were used in each test. Experiments were conducted in triplicate (n = 27).

The Microtox® bioassay was used to measure the acute toxicity of the PAHs' supernatant samples after yeast treatment, based on changes of luminescence of the bacterium *Aliivibrio fischeri* (Microtox® Model 500 Toxicity Analyzer, Analytic Instrumentation S.A. Madrid, Spain). The toxicity was expressed as the concentration that causes a 50% light reduction of *A. fischeri* after 5 and 15 min of exposure (EC50), according to published protocols (Qureshi et al., 1982; Guisado et al., 2016).

Toxicity after yeast treatment was also analyzed using red blood human cells and pulmonary epithelial cells (cell line A549) according to Lackey et al. (1999) and Uliasz et al. (2000) respectively. Erythrocyte hemolysis and dead pulmonary cells (expressed in percentages) were determined after a whole blood sample and the cell line A549 were exposed to treated and non-treated supernatants by *R. mucilaginosa* EXF-1630. Resulting cellular changes were observed by microscopy. The smear of blood human cells was observed using a bright-field microscope (Zeiss Corp., Thornwood, New York, U.S.), while pulmonary epithelial cells were observed using an inverted microscope (Zeiss Corp., Thornwood, New York, U.S.). In all experiments, negative and positive controls were implemented as described above. Experiments were performed in triplicates and three experimental determinations were made for each sample (n = 9).

2.6. Metabolic profiling studies in Rhodotorula mucilaginosa EXF-1630 during polycyclic aromatic hydrocarbon biodegradation at hypersaline conditions

Metabolites were extracted from 10 mL of supernatant samples. Three equal volumes of MS grade ethyl acetate were added and the solvent was removed using a rotary evaporator at 40 °C. Samples were concentrated in 1 mL of MS grade methanol (Wunder et al., 1997). For extraction of intracellular metabolites, yeast cells were resuspended in 3 mL of MS grade water until their complete homogenization, followed by sonication for 10 min. Lysis Matrix E tubes (MP Biomedicals™, California, U.S., Catalogue 116914050-CF) and a FastPrep-24™ 5G homogenizer (MP Biomedicals™, California, U.S.) were used to disrupt cell walls and cytoplasmic membranes. After that, 2 mL of the lysed cell samples were mixed with 10 mL of MS grade acetone for 20 min. After adjusting to pH 2.0 (using 1 N HCl), samples were sonicated for 10 min and centrifuged at 14,000 × *g* for 10 min. The solvent was removed using a rotary evaporator, and samples were collected as described earlier, using 1 mL of methanol (Wunder et al., 1997).

The experiment was performed in triplicates and three experimental determinations were made for each sample (n = 9).

Chromatographic analysis of the metabolites was made using a UHPLC Acquity I-Class System (Waters, Milford, U.S.) connected to a Synapt-G2-HDMS mass spectrometer (Waters, Milford, U.S.). A Waters Cortecs® C-18 2.7 μm column (100 mm; Waters, Milford, U.S.) was used. The method conditions included a mobile phase A: H_2O with 0.1% NH_3 and B: acetonitrile with 0.1% ammonia, in a gradient flow rate of 0.350 L/min (initial 0% B; 5 min 70% B; 5,1 min 100% B; 6,6 min 0% B; 10 min 0% B) with 10 min as the run time. The column temperature was set at 40 °C and 5 μL of each sample was injected. Z-Spray electrospray ionization interface was working in negative (ESI-) and positive ion (ESI+) mode with reference capillary voltages at 2.1 kV and 2.5 kV, respectively. The source temperature was set at 100 °C and the desolvation temperature at 500 °C. The spectrum analysis, the analysis of the metabolites, the m/z value, and error calculation, as well as the control of the equipment, was made by the MassLynx software (version 4.1, Waters Milford, U.S.). The m/z value of each ion mass was used to retrieve metabolites using the online databases and bibliography previously reported with the following parameters: Mass Chromatogram Window 10.0 ppm, mass tolerance 30 ppm, and Monoisotopic Mass Mode for the structure prediction.

2.7. Transcriptomic of Rhodotorula mucilaginosa EXF-1630 during polycyclic aromatic hydrocarbon biodepletion at hypersaline conditions

Three-day-old cultures of *R. mucilaginosa* in the presence of Phe and BaP (1:1, 100 ppm final concentration) or 2% glucose (control) at hypersaline conditions (1 M NaCl) were obtained. Cells were collected as previously described, and ground in liquid nitrogen. Total RNA was isolated using the TRIzol extraction method (Thermo Fisher Co., U.S., 15596026), and a quality check (RNA integrity number (RIN) > 7) was performed with the Agilent 2100 Bioanalyzer. The samples were subject to rRNA depletion followed by fragmentation, first- and second-strand cDNA synthesis, adenylation of 3′ ends, adapter ligation, DNA fragmentation enrichment, and real-time PCR quantification. Samples were sequenced (2 × 150 bp paired-end) on the Illumina HiSeq-2500 platform by ABM Company (Vancouver, Canada). Three replicates were sequenced for each study condition (n = 3).

After demultiplexing, sequences were processed to remove low-quality reads and trimmed to remove adaptors using Trimmomatic version 0.39 (Bolger et al., 2014). Highly overrepresented sequence reads were eliminated using a custom python script (https://github.com/harvardinformatics/TranscriptomeAssemblyTools/blob/master/RemoveFastqcOverrepSequenceReads.py). Read sequencing errors were converted to the most probable nucleotide using Rcorrector (Song and Florea, 2015). The resulting sequence reads from each sample were pooled to perform *de novo* transcriptome assembly using Trinity version 2.10.0 (Grabherr et al., 2011). Transcriptome quality was estimated by assessing completeness using BUSCO version 4.0.5 (Seppey et al., 2019). Functional annotation of the predicted transcripts was carried out using Blast2GO in OmicsBox (Biobam Bioinformatics, 2019). Briefly, a blast search against the Fungi section in the nr database was conducted and gene ontology (GOs) were transferred from resulting hits. InterPro annotations were also retrieved and GOs merged with the previous annotation.

Transcript abundance estimation was conducted using Kallisto v0.46.1 (Bray et al., 2016). Estimated read counts were normalized using RUVseq (Risso et al., 2014) and differential expression analysis was conducted using DESeq2 version 1.29.5 (Love et al., 2014). The set of differentially expressed transcripts was used for GO enrichment using Blast2GO in OmicsBox (Biobam Bioinformatics, 2019). Blast2GO uses over-representation analysis to estimate the false discovery rate (FDR) of GO enrichment using a Fisher's Exact Test. Pathway enrichment analysis based on KEGG mapper (Kyoto Encyclopedia of Genes and Genomes) was conducted using the KEGG annotations obtained by GhostKOALA (Kanehisa and Sato, 2020).

Transcriptomic data is publically available in the National Centre for Biotechnology Information (NCBI): Submission ID: SUB8068200, BioProject SRA ID: PRJNA660798, BioSample accession: SAMN15961492.

2.8. Genomic analysis of xenobiotics metabolism and biodegradation in yeasts

Sixty-one yeast genomes deposited in the MycoCosm database (https://mycocosm.jgi.doe.gov/mycocosm/home) were analyzed and the number of genes annotated to 31 KEGG biological processes related to xenobiotic degradation was identified (Supplementary Material Table S1) (Kanehisa and Sato, 2020).

The number of enzyme coding genes in each pathway was used for clustering analysis by the UPGMA method using Jaccard distance. A heatmap showing normalized values was obtained using the vegan package in R (Oksanen et al., 2007). Besides, a non-metrical multidimensional scaling analysis (NMDS) was performed to reduce the data to a three-dimension space without value autotransformation using the global model in the monoMDS function of the vegan package.

2.9. Statistical calculations

Simple ANOVA tests were performed to determine statistically significant differences in data ($p < 0.05$). Hartley-Cochran-Bartlett and Kolmogorov-Smirnov tests were conducted to test the variance homogeneity and the normal distribution of data. A post hoc analysis (Tukey HSD and Duncan tests) was used to establish the order of the ANOVA differences. Figures show the average of at least three replicates and the standard deviations. All statistical calculations were made on GraphPad version Prism8 (https://www.graphpad.com). In particular, statistical determinations related to transcriptomic studies were performed using R (R Core Team, 2020).

3. Results and discussion

3.1. Polyphasic identification of Rhodotorula mucilaginosa EXF-1630

Phylogenetic reconstruction of the strain EXF-1630 isolated from Arctic sea ice in Kongsfjorden, Ny-Alesund, Svalbard (Norway) shows that EXF-1630 was placed unambiguously in the *R. mucilaginosa* cluster with high branch support (Supplementary Material Fig. 1). The phylogeny based on a multiple sequence alignment of concatenated 24 highly conserved markers (Ren et al., 2016), clearly revealed the taxonomic position. *R. mucilaginosa* EXF-1630 was closely related to *R. mucilaginosa* CYJ03, a psychrotolerant and halotolerant yeast isolated from water of the northern Yellow Sea of China (Tang et al., 2020).

EXF-1630 produced red/orange colored colonies on YNG (Fig. 1A), Sabouraud and Malt Extract agar media (data not shown). This pigmentation is a distinctive characteristic of the genus *Rhodotorula* that supports its taxonomic allocation (Harrison, 1928; Wang et al., 2016; Tang et al., 2020). The minimal medium used in this study inhibited the carotenoid synthesis as evidenced by the loss of pigmentation (Fig. 1B). Microscopic characterization showed that EXF-1630 is a unicellular budding yeast (no teleomorph was found under the tested conditions), ovoid, and strictly aerobic. A

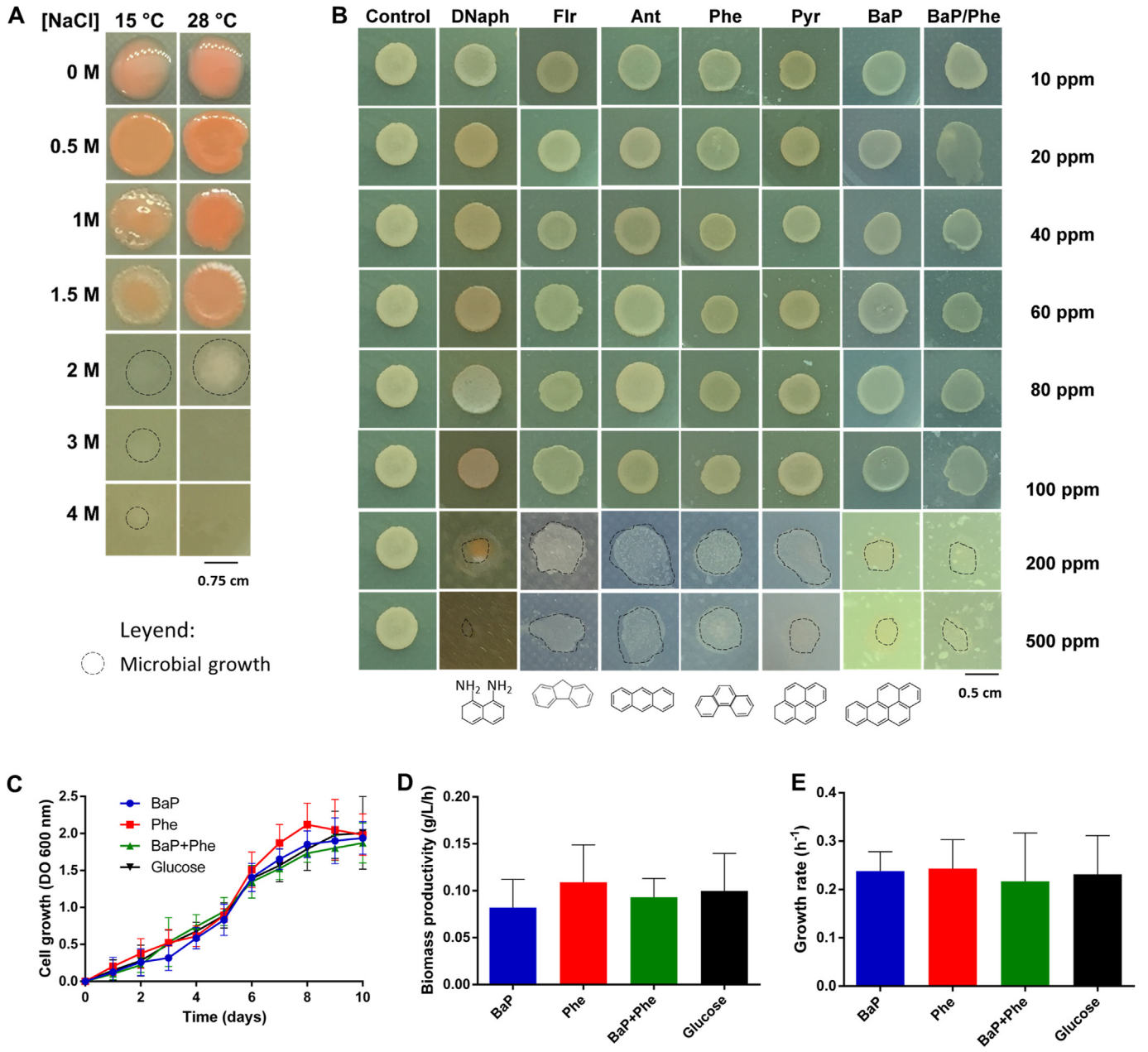

Fig. 1. A) Growth of *Rhodotorula mucilaginosa* EXF-1630 on YNB agar medium at different NaCl concentrations at 15 and 28 °C. Broken circles represent weak growth of the yeast strain in some salt concentrations. B) Growth of *R. mucilaginosa* EXF-1630 on hypersaline (1 M NaCl) minimal medium supplemented with glucose (control), 1,8 diaminonaphthalene (DNaph), fluorene (Flr), anthracene (Ant), phenanthrene (Phe), pyrene (Pyr), benzo[a]pyrene (BaP), or a mixture of Phe and BaP (1:1) as only carbon sources. Different final concentrations were used: 10, 20, 40, 60, 80, 100, 200, and 500 ppm. C) Cell growth ($OD_{600\ nm}$), D) biomass productivity, and E) growth rate of strain EXF-1630 cultured in hypersaline liquid medium with glucose (control), Phe, BaP, or a mixture of both aromatic compounds (1:1, 100 ppm final concentration) as only carbon source. Polyaromatic compounds were added at 100 ppm at final concentration in all cases.

polyphasic taxonomy approach of EXF-1630 based on phylogenetic markers ITS, LSU, SSU, EF1, CYTB, micro-, macro-morphological, and physiological characteristics (Biolog microplates) confirmed the molecular identification (data not shown).

Some *R. mucilaginosa* strains have been considered as opportunistic pathogens that affect mainly immunocompromised individuals, but rarely infect healthy individuals (Wirth and Goldani, 2012; Jarros et al., 2020). A strong body of evidence supports that invasive events are associated with *(i)* the use of broad-spectrum antibiotics, *(ii)* nosocomial environments and *(iii)* preconditioned patients (patients with central venous catheter, solid and hematologic malignant tumors or AIDS) (Wirth and Goldani, 2012). The strain EXF-1630, isolated from a cryophilic environment, shares major genomic-functional traits with environmental ecotypes (plant endophytes, carotenoids, and oils producing), and is genomically divergent from strains related to pathogenesis (Supplementary Material Fig. 2). The strain EXF-1630 shares lineage with other cryophilic extremophile strains, and ecotype that is poorly adapted to high basal temperature sustained in humans. A common trait in pathogenic strains is their ability to grow around 37 °C (as occur in *Candida* species). In any case, the use of *R. mucilaginosa* in environmental remediation treatment processes should be carefully analyzed, and tests should be performed before using strains of this species for industrial or environmental

purposes, especially regarding those of pathogenicity to mammals.

3.2. *Rhodotorula mucilaginosa EXF-1630 is a halotolerant yeast able to grow on a wide variety of polycyclic aromatic hydrocarbons as sole carbon sources*

R. mucilaginosa EXF-1630 grew as red/orange pigmented colonies at 1 M NaCl at both 15 °C and 28 °C (Fig. 1A). EXF-1630 did not show growth at 37 °C. High salt concentrations (>1.5 M NaCl) negatively influenced pigment production. Growth at 2 M NaCl was weaker at 15 °C than at 28 °C, while no growth was detected at higher NaCl concentrations at 28 °C.

R. mucilaginosa, a saprophytic basidiomycetous yeast (family Sporidiobolaceae), is widely distributed in nature (Wang et al., 2016), even in different hypersaline and extremely cold environments, such as salterns, hypersaline lakes, Antarctic and Arctic coasts, snow, sea ice and glacial ice (Gunde-Cimerman et al., 2005; de Menezes et al., 2019; Perini et al., 2019; Rafiq et al., 2019; Zajc et al., 2019). Yeasts adapted to both, high salt and low-temperature share several physiological adaptations, related to life at low water activities. Adaptive fungal strategies to endure low temperature and salt stress seem to be closely related (Gunde-Cimerman et al., 2005; Collins and Margesin, 2019). *R. mucilaginosa* EXF-1630 isolated from Arctic sea ice displayed both a halotolerant and psychrotolerant behavior (Fig. 1A). *R. mucilaginosa* strains also often colonize highly polluted toxic environments, such as heavy metal-contaminated mine drainage wastes, oil- and polyaromatic compounds-contaminated soils, water effluents from olive mills, and municipal wastes, among others (Chandran and Das, 2012; Irazusta et al., 2012; Ilyas et al., 2016; Liu et al., 2017; Hesham et al., 2018; Mikolasch et al., 2019; Zajc et al., 2019). *R. mucilaginosa* strains were recognized for their potent biodegradation pathways of xenobiotics metabolism and ability to grow on concentrated cytotoxic chemicals (Addis et al., 2016). Many anthropogenically polluted environments are additionally inhibitive, due to various extreme conditions, including the presence of contaminants. Polyextremotolerant strains of *R. mucilaginosa* can adapt to a broad range of pH, temperatures (0.5–37 °C), high levels of ionizing radiation, oxidative stress, tolerance to multiple heavy metals (e.g. Ni, Cd, Cr, Cu, Hg), and oligotrophic conditions (Addis et al., 2016; Liu et al., 2017; Tkavc et al., 2018; Zajc et al., 2019; Ide-Pérez et al., 2020). Thus, *R. mucilaginosa* has emerged as a promising non-conventional yeast with attractive features for xenobiotics biodepletion under harsh environmental conditions (Deligios et al., 2015; Addis et al., 2016).

In the present study, we focused on *R. mucilaginosa* EXF-1630, exposed to PAHs as sole carbon sources at hypersaline conditions (1 M NaCl). A preliminary screening showed its ability to successfully grow on a structurally diverse group of polyaromatic compounds (Fig. 1B). Surprisingly, PAHs supported growth as well as glucose, even at high PAHs concentrations (e.g. 100 ppm), extremely toxic to most cells. It grew up to 500 ppm of the tested PAHs at hypersaline conditions. At 200 and 500 ppm of PAHs, yeast colonies were scattered and had irregular contours (Fig. 1B). EXF-1630 assimilated 1,8 diaminonaphthalene, an NH_2-substituted PAH recalcitrant to biodegradation (Varjani, 2017; Srivastava and Kumar, 2019), and it also grew on a mixture of Phe and BaP at different final concentrations (Fig. 1B). The potential utility of EXF-1630 in bioremediation was also highlighted by its ability to assimilate a set of PAHs with different hydrophobic properties at hypersaline conditions. Thus, EXF-1630 could be regarded as of polyextremotolerant nature since it is halotolerant, psychrotolerant, and tolerant to xenobiotics.

Based on these results, the growth kinetic of EXF-1630 in hypersaline (1 M NaCl) liquid medium supplemented with either Phe, BaP, or the mixture of the two (Fig. 1C) and the biomass productivity and growth rates were determined (Fig. 1D and E). Phe and BaP have been recognized as low- and high-weight model PAHs that contain three- and five-benzene rings, respectively (Varjani, 2017; Srivastava and Kumar, 2019). The angular arrangement of their aromatic rings imposes a severe restriction on the biodegradative processes in comparison with PAHs with linear topology (Srivastava and Kumar, 2019). The selected PAHs are also considered model polyaromatic compounds because they induce high levels of oxidative stress in various life forms (Varjani, 2017; Srivastava and Kumar, 2019).

Cell growth was not different when *R. mucilaginosa* EXF-1630 grew on either PAHs or glucose as sole carbon source after 10 days of culture (Fig. 1C). The fact that EXF-1630 can indistinctly assimilate glucose or PAHs (Fig. 1B and C) was further supported by the lack of an initial adaptation phase (lag phase) when it was cultured on Phe. Growth on Phe was slightly better than on BaP, glucose, or the mixture of both PAHs at day seven and eight. Biomass productivity and growth rates were similar at all the studied conditions with no statistically significant differences among them (Fig. 1D and E).

EXF-1630 had similar biomass productivity in the presence of Phe, BaP, or a mixture of both. Similar results have been previously observed for *R. taiwanensis, R. ingeniosa, Candida pseudointermedia,* and *Yamadazyma mexicana* exposed to octane and pyrene (Hashem et al., 2018). The growth rates of EXF-1630 at the studied conditions were similar to values reported for a wastewater-derived *R. mucilaginosa* grown in presence of phenolic compounds (Jarboui et al., 2012). A recent screening of the assimilation of six aromatic compounds by 36 yeasts found that the highest absorbance at 600 nm was 0.5, a much lower value than the one attained by EXF-1630 (Fig. 1C) (Yaguchi et al., 2020). The same study also demonstrated that in many yeasts (e.g. *R. araucariae, R. borgoiensis, R. dairenensis, R. mucilaginosa, R. graminis, Rhodosporidiobolus ruineniae, Solicoccozyme phenolicus, Sporobolomyces johnsonii, Occultifur extemus, Yarrowia lipolytica*) the same biomass density was obtained in the presence of certain aromatic compounds as in glucose, as corroborated by our observations (Fig. 1D and E).

R. mucilaginosa has been extensively studied for its ability to deplete persistent anthropogenic pollutants such as PAHs, phenols, dimethyl phthalates esters, and heavy metals (Jarboui et al., 2012; Irazusta et al., 2012; Wang et al., 2013, 2016a; Hesham et al., 2018; Belloch et al., 2020). Recently, an *R. mucilaginosa* strain isolated from subsoil groundwater contaminated by hydrocarbons showed a high capacity to degrade naphthalene, fluorene, and octane (Belloch et al., 2020), while another strain (KKU-A29) was efficient in transforming toluene (Hesham et al., 2018). Another *R. mucilaginosa* strain isolated from oil mill wastewater could efficiently assimilate phenolic substrates (e.g. tyrosol, gallic acid, vanillic acid, *p*-coumaric acid, and protocatechuic acid) (Jarboui et al., 2012). However, not all *R. mucilaginosa* strains can equally metabolize aromatic compounds. For example, *R. mucilaginosa* CBS 349 isolated from smut-infected leaves poorly metabolized syringate and ferulate (Yaguchi et al., 2020).

R. mucilaginosa EXF-1630 cells formed muriform clumps in the presence of PAHs (Fig. 2A–C). More budding cells were observed in the culture medium with Phe, in comparison to BaP or glucose (Table 1). Polyaromatic hydrocarbons did not significantly affect neither cell size nor general morphology when compared to growth on glucose, in contrast to increased cells of *Rhodosporidium kratochvilovae* and *Cryptococcus psychrotolerans* when exposed to (poly)aromatic compounds (Patel et al., 2017; Deeba et al., 2018).

The biophysical characterization of the *R. mucilaginosa* EXF-1630 cultures showed that the hydrodynamic radius and the polydispersity index largely changed during the experiment

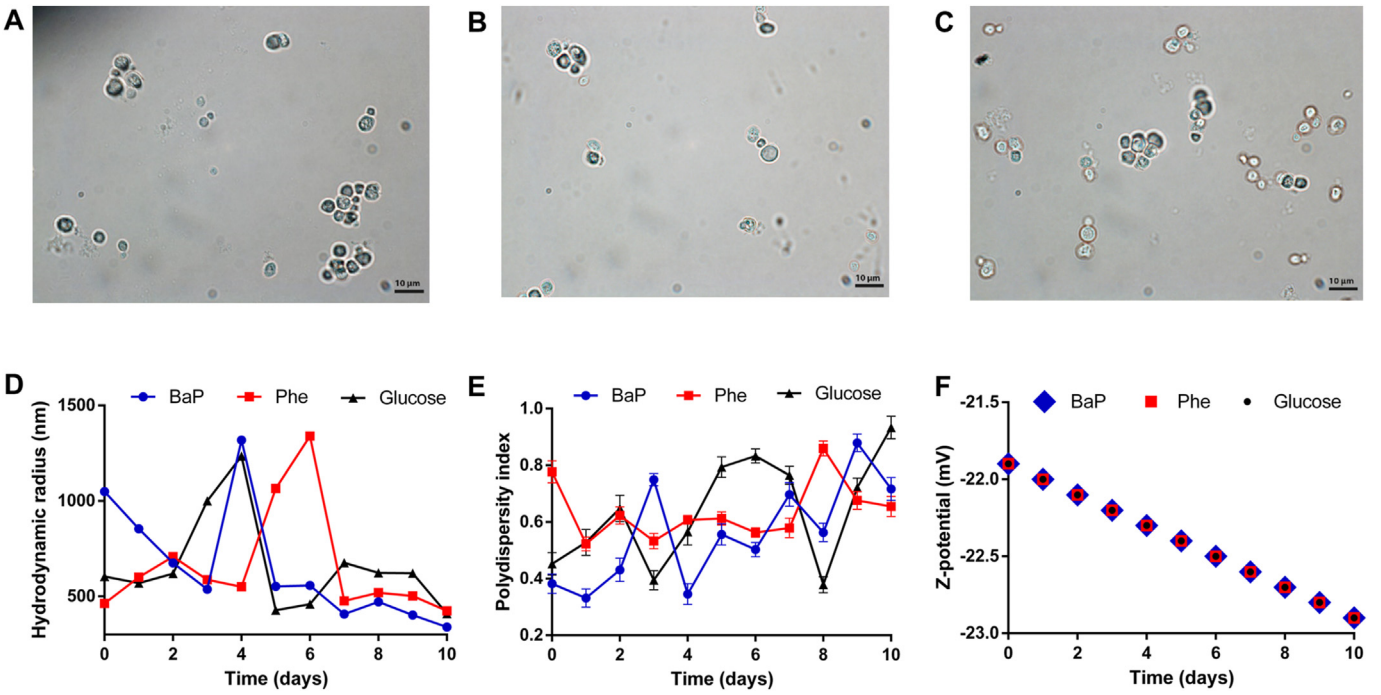

Fig. 2. A, B and C) Microscopic preparations of EXF-1630 in the presence of phenanthrene (Phe), benzo[a]pyrene (BaP), or a mixture of both (1:1, 100 ppm final concentration) after three days exposure time at 1 M NaCl. D, E and F) Changes of hydrodynamic radius, polydispersity index, and Z-potential during Phe and BaP removal, respectively.

Table 1
Microscopic characterization of *Rhodotorula mucilaginosa* EXF-1630 during PAH exposure at hypersaline conditions.

Condition	Cells/μL	Budding cells/μL	Diameter (μm)	Cell area (μm^2)
Glucose (control)	41.3 ± 12.4	14.8 ± 3.1	5.6 ± 0.7	24.9 ± 5.6
Phenanthrene (Phe)	56.8 ± 4.6	27.8 ± 6.3	4.8 ± 0.8	20.2 ± 5.4
Benzo [a] pyrene (BaP)	31.3 ± 3.6	10.5 ± 2.1	5.2 ± 0.9	25.3 ± 6.4
Phe + BaP	38.8 ± 5.7	21.4 ± 4.3	4.7 ± 0.6	18.6 ± 4.6

PAHs were added at 100 ppm as final concentration.
Mixture of Phe and BaP (1:1) was prepared by adding 50 ppm of each polyaromatic hydrocarbon.

(Fig. 2D and E). The variations in the hydrodynamic radius could be due to the very heterogeneous cellular suspensions due to muriform clumps in all studied conditions (Fig. 2A, B and C). The polydispersity index showed a slight tendency to increase over time. This could be due to the increase in cell density and the clumped yeasts. No specific tendency was observed for both parameters. In contrast, Z-potential clearly showed a lineal decrease during the 10 days (Fig. 2F).

These experiments suggest that the cellular system is not homogeneously distributed in the studied conditions. Probably, the irregular muriform clumps influence the large variations of the hydrodynamic radius and polydispersity index. Since Phe and BaP did not affect the electrokinetic potential of cells or their dimensions in comparison with glucose, no extensive modifications of the cell wall structure occurred, which could be important to keep ion homeostasis in these hydrophobic substrates (Fig. 2F).

3.3. Biodegradation of phenanthrene and benzo[a]pyrene by *Rhodotorula mucilaginosa* EXF-1630 under hypersaline conditions

Based on the demonstrated ability of *R. mucilaginosa* EXF-1630 to grow in presence of mixtures of Phe and BaP, we evaluated their removal in 1 M NaCl liquid media supplemented with both PAHs as the sole carbon sources. After two days of exposure, 30 and 40% of Phe and BaP, respectively, were adsorbed (Fig. 3A). Later, EXF-1630 preferentially adsorbed BaP over Phe, and the biodegradation processes prevailed over bioadsorption (Fig. 3A and B), which notably contributed to PAH removal in the early stages. BaP, a five-rings PAH, was preferably adsorbed possibly due to a higher hydrophobicity/lipophilicity in comparison with Phe (three-rings PAH) (Alegbeleye et al., 2017; Srivastava and Kumar, 2019). Significant levels of biodegradation were observed from the beginning of the experiment (Fig. 3B), resulting in 40% biodegradation of each PAH on the second day and 80% after 10 days (Fig. 3A). Bioadsorption in parallel drastically decreased (four-fold) in 10 days, diminishing to 20% at the end of the experiment (Fig. 3A). Degradation of Phe and BaP were similar at different days with no significant differences ($p < 0.05$) found between biodegradation percentages at different days (Fig. 3B). In our group, we have found similar results in other PAH degrader fungi such as *Aspergillus sydowii* (Peidro-Guzmán et al., 2020), *Exophiala* sp. (Ide-Pérez et al., 2020), or even other *R. mucilaginosa* strains, where Phe and BaP degradation kinetics are similar. This could be the result of low specificity enzymes involved in the mineralization pathways of both compounds, but further experiments should be conducted to test this statament. Biodegradation was exponential between 0 and 6 days ($R^2 = 0.997$ -nonlinear regression (curve fit) exponential, confidence interval: 95%). Both chemical oxygen demand (COD) and pH drastically decreased already after two days of culture (Fig. 3C), resulting in a 99.4% reduction of COD after 10 days.

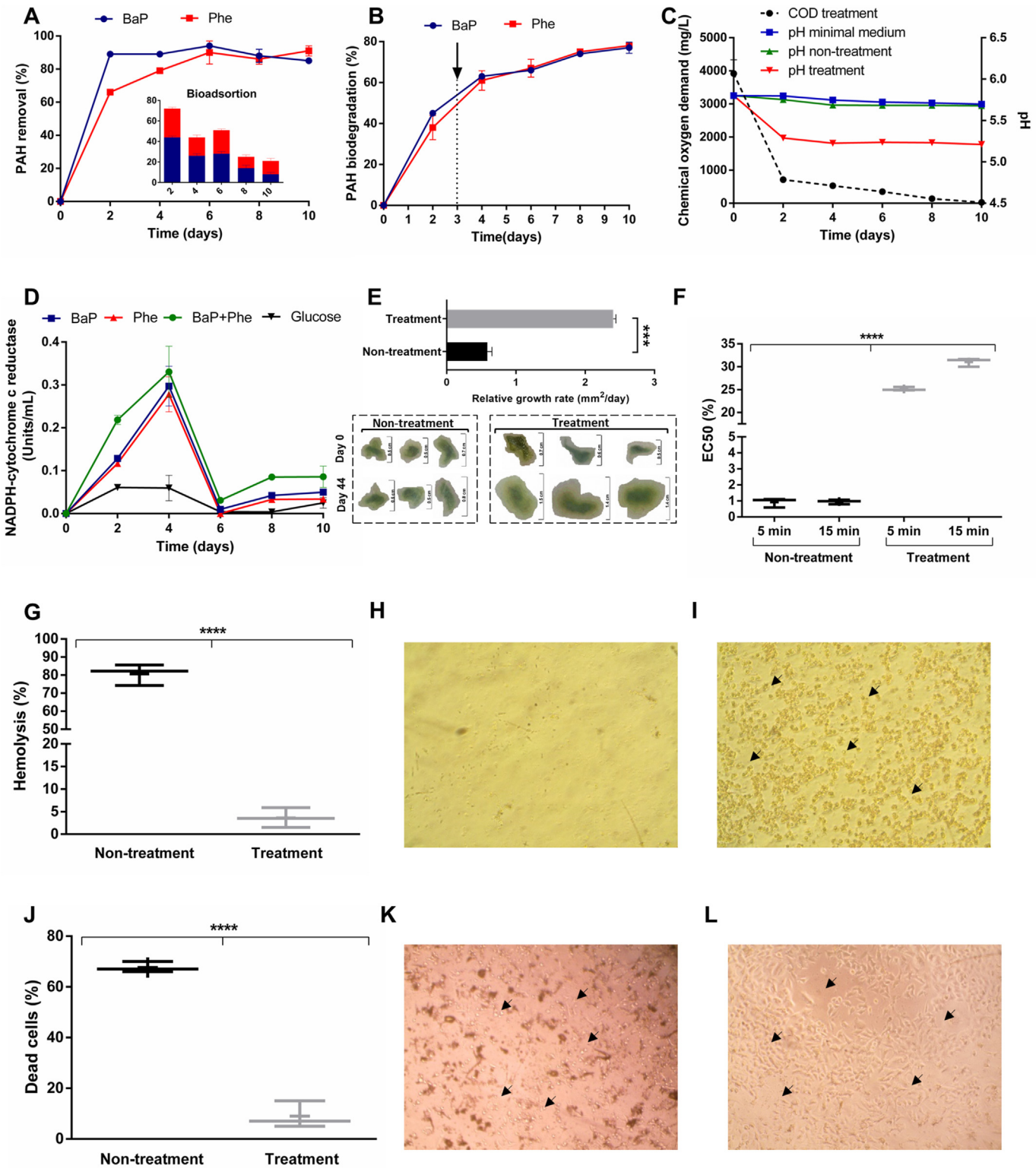

Fig. 3. A and B) Removal, bioadsorption, and biodegradation of phenanthrene (Phe) and benzo[a]pyrene (BaP) by *Rhodotorula mucilaginosa* EXF-1630 at hypersaline conditions (1 M NaCl). Polyaromatic hydrocarbons (1:1) were added at 100 ppm as total final concentration. C) Chemical oxygen demand (COD) and pH variation during Phe and BaP removal. D) NADPH-cytochrome *c* reductase activity during 10 days of aromatic compound exposure. E) Relative growth of *Physcomitrium patens* (previously named *Physcomitrella patens*) when moss was grown in presence of supernatants from treated and non-treated PAHs polluted media. F) Toxicological tests on the bioluminescence bacteria *Aliivibrio fischeri*. G) Hemolitytic assay on red human blood cells using treated and non-treated PAHs polluted media. H and I) Microscopy of hemolytic assays using pelleted cells in the presence of supernatants from treated and non-treated PAHs polluted media. J) Cellular viability assay using Trypan Blue stain of pulmonary ephitelial cell line (A549). K and L) Microscopy of pulmonary ephitelial cell line (A549) after 24 h cultured in the presence of supernatants from treated and non-treated PAHs polluted media. Black arrows depict red blood cells (Fig. 4I), and pulmonary cells with cellular damages or normal morphology, respectively (Fig. 4K and L). Representative microscopic images were selected. Asterisks represent statistically significant differences (Duncan test, $p < 0.05$). (For interpretation of the references to color in this figure legend, the reader is referred to the Web version of this article.)

In parallel, enzymatic activities typically involved in PAH biodegradation were measured. Extracellular laccase, peroxidase, and un-specific peroxygenase activities were not detected during the experiment. In contrast, NADPH-cytochrome *c* reductase activity was observed and reached its maximum at day four, drastically decreased at day six, and remained low until the end of the experiment (Fig. 3D).

The biochemical characterization of the Phe and BaP removal highlighted the potential of *R. mucilaginosa* EXF-1630 as a bioremediating agent under saline conditions. EXF-1630 biodegraded the complex polyaromatic mixture of both PAHs to the same high extent, accompanied by a significant reduction of COD, a trait strongly desired in bioremediation processes (Srivastava and Kumar, 2019). High salinity (1 M NaCl) did not reduce the removal of Phe and BaP, even though low water activity negatively affects the bioavailability of PAHs (McGenity, 2016; Varjani, 2017).

R. mucilaginosa EXF-1630 was more successful in removing selected PAHs in comparison to the removal of anthracene, naphthalene, and BaP by the black yeast *Aureobasidium pullulans* exposed at 90 ppm (Leelaruji et al., 2013), Phe and BaP by *Pichia anomala* (Hesham et al., 2006) and *Candida tropicalis, C. viswanathii,* and *Rhodotorula* sp. NS01 (Hesham et al., 2009; Farag and Soliman, 2011; Kumar and Nilanjana, 2017). For example, *C. viswanathii* removed 55% of BaP after 10 days in mixtures of PAHs at 7.6 ppm (Hesham et al., 2009), while *Rhodotorula* spp. NS01 assimilated 50% of 10 ppm of BaP in seven days (Kumar and Nilanjana, 2017). *C. viswanathii* strains degraded 77% of Phe in 10 days from a solution containing 7.6 ppm of a misture of PAHs (Hesham et al., 2009), similar to results obtained with *C. psychrotolerans* cultured in the presence of naphthalene, anthracene, and pyrene at 1.25 g/L (Deeba et al., 2018) and to results obtained by *R. mucilaginosa* EXF-1630.

The PAHs degradation by halotolerant yeasts in saline conditions has been poorly studied (Hadibarata et al., 2017; Kamyabi et al., 2018). Exceptions represent the halotolerant yeast *Basidioascus persicus* EBL-C16 that successfully removed anthracene, pyrene, and Phe in 21 days at 2.5% NaCl (Kamyabi et al., 2018) and *Candida* sp. S1 that degrade up to 75% of 20 ppm of these PAHs in presence of 2.4% of NaCl (Hadibarata et al., 2017). While the hydrocarbon removal efficiency and the biomass productivity reached by both *B. persicus* and *Candida* sp. S1 are similar to those obtained by EXF-1630, our strain achieved this biodegradation within 10 days from cultures with higher concentrations of PAHs (100 ppm) (Fig. 3A and B).

The successful removal of PAHs and the absence of toxic metabolites related to biodegradation were corroborated by toxicological tests (Fig. 3E-L). Explants of the moss *P. patens* grown in yeast-treated PAHs polluted media even showed a five-fold increase in growth rate in comparison to negative controls (Fig. 3E). The same trend was confirmed in the microtox assay using a marine bioluminescent bacterium *A. fischeri* (Fig. 3F). Toxic compounds strongly inhibit its cellular respiration and impair bioluminescence (Girotti et al., 2007). Exposure to yeast-treated PAHs polluted media (5-and 15-min) resulted in less disrupted luminescence than in the negative control (Fig. 3F). Red blood human cells and pulmonary epithelial cells (cell line A549) were also used to toxicologically validate the bioremediating potential of *R. mucilaginosa* EXF-1630 (Fig. 3G-L). Although PAHs have a strong hemolytic effect on red blood cells (Fig. 3G and H), hemolysis decreased by 80% when they were incubated with EXF-1630 (Fig. 3G). Microscopic analysis confirmed lysis of erythrocytes by the PAHs recovered from polluted media (Fig. 3H), whereas erythrocytes exposed to extracts obtained from yeast-treated media remained almost unaffected (Fig. 3I). Exposure of pulmonary epithelial cells (A549) to PAHs polluted media (Fig. 3J-L) caused lethality of up to 70% of the cells, in comparison to 7% when incubated with mycoremediated media (Fig. 3J). Lethal effects were confirmed by microscopic observations, characterized by drastically affected cell morphology in the presence of non-treated PAHs polluted media (Fig. 3K and L).

To summarize, our results demonstrate that *R. mucilaginosa* EXF-1630 is an excellent candidate to mitigate PAH pollution in hypersaline conditions (Fig. 3A-L). It not only can successfully degrade PAHs but is also able to significantly decrease the toxicity of the resulting media (Fig. 3E-L), as shown by four models: a bacterium, a plant, and two types of human cells. Mycotreatments with EXF-1630 thus represent an attractive option for biotechnological applications, in particular under real field conditions.

3.4. Metabolic profile of Rhodotorula mucilaginosa EXF-1630 during PAHs biodegradation under hypersaline conditions

The metabolic profile was determined after three days of culture in a medium with Phe and BaP at 100 ppm final concentration and with 1 M NaCl added. Three days represented the midpoint of the biodegradation exponential phase (Fig. 3B), which lasted from 0 to 6 days of treatment ($R^2 = 0.997$).

Twelve metabolites were identified as by-products from Phe and BaP degradation by *R. mucilaginosa* EXF-1630 (Table 2). They included different hydroxylated products both in the supernatant as well as inside the cells (Table 2). Hydroxy-benzo[α]pyrene, 9,10-dihydroxyphenanthrene, phenanthrene trans 9,10-dihydrodiol, 9-phenanthrol, and dihydroxy-benzene were found in the culture medium, probably as the result of the cytochrome P450 monooxygenase activity (Kashyap et al., 2020). These metabolites have been frequently reported during PAHs degradation by fungi (Cerniglia 1997; Hashem et al., 2018; Fu et al., 2018; Peidro-Guzmán et al., 2020).

The conjugative metabolite 1-phenanthryl-β-D-glucopyranose was detected both in the culture medium as well as in the cells, indicating the presence of intracellular glycosyl-transferases functionally active during PAHs biodegradation. This metabolite has been also found in *Cunninghamela elegans* exposed to PAHs (Casillas et al., 1996).

Although the extracellular presence of these metabolites suggests specific putative membrane transporters facilitating PAHs translocation their occurrence is still poorly understood. Some major facilitator superfamily (MFS) transporters and ATP-binding cassette (ABC) transporters seem to play a key role in mediating the influx and efflux of PAHs and by-products across the cell membranes (Verdin et al., 2005; Park et al., 2019).

The putative presence of quinones such as phenanthrene-1(2H)-one, could indicate the participation of oxidoreductases and the presence of hydroxynaphtoic acid and phthalic acid could indicate a different biodegradation mechanism than in some filamentous fungi (Aranda et al., 2017). The PAHs degradation via phthalic acid pathway has been previously reported for the halotolerant yeast *B. persicus* (Kamyabi et al., 2018) and deep-sea isolate of *R. mucilaginosa* Mar-Y3 during dimethyl phthalate degradation. Dimethyl isophthalate and dimethyl terephthalate were degraded via terephthalic acid (Wang et al., 2016). Other phthalate derivatives were identified in the cell-free extract of *R. taiwanensis* HKUY-0162 grown with octane as the sole carbon source (Hashem et al., 2018). These studies demonstrated that phthalic acid is an important metabolite in the catabolic pathway of PAHs in yeasts.

Benzo[a]pyrene ring cleavage occurs via *meta*-oxidation leading to the formation of 2-hidroxymuconic semialdehyde pyrene, indicating the possible participation of catechol 2,3-dioxygenase enzymes. This metabolite has been found also in the yeast *C. tropicalis* during pyrene degradation, possibly after cleavage of R-catechol via *meta*-fission pathway to 2-hydroxy muconic (Kashyap et al., 2020).

Table 2
Metabolites in the culture medium and inside the cells of *Rhodotorula mucilaginosa* EXF-1630 after degradation of phenanthrene and benzo[α]pyrene under hypersaline conditions by UPLC-QTOF-MS in positive and negative mode after three days of cultivation.

m/z	Metabolite	Chemical composition	Sample	Error (ppm)	Retention time (min)	Structure
357.1354 [M+H]	1-Phenanthryl β-D-glucopyranose	$C_{20}H_{20}O_6$	Pellet Supernatant	4.5	1.872	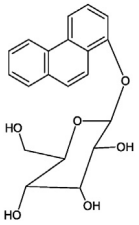
331.0882 [M+H]	2-Hydroxymuconic semi aldehyde pyrene	$C_{21}H_{14}O_4$	Pellet	−26.6	4.80	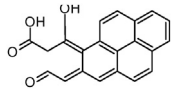
293.3200 [M-H]	Phenanthrene trans 9,10-dihydrodiol sulfate	$C_{14}H_{13}O_5S$	Pellet	17.0	2.071	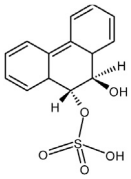
269.0966 [M+H]	Hydroxy-benzo[α]pyrene	$C_{20}H_{12}O$	Pellet Supernatant	5.9	1.38	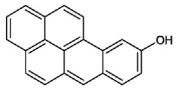
213.0916 [M+H] 211.0759 [M-H]	Phenanthrene trans 9,10-dihydrodiol	$C_{14}H_{12}O_2$	Supernatant	−6.1 0.5	0.52 7.524	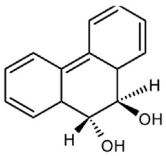
209.0600 [M-H]	9,10-Dihydroxyphenanthrene	$C_{14}H_{10}O_2$	Supernatant	−1.4	0.151	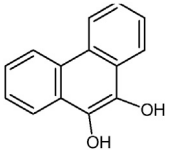
195.0810 [M+H]	9-Phenanthrol	$C_{14}H_{10}O$	Supernatant	−10.3	0.7	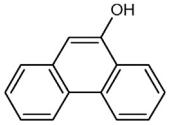
195.08100600 [M+H]	Phenanthrene-1(2H)-one	$C_{14}H_{10}O$	Supernatant	−1.5	0.72	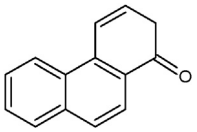
188.047 [M+H] 187.0424 [M-H]	Hydroxy-naphtoic acid	$C_{11}H_8O_3$	Pellet Supernatant	3.2 15.5	0.424 0.578	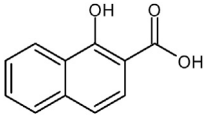
167.0344 [M+H] 165.0188 [M-H]	Phthalic acid	$C_8H_6O_4$	Pellet Supernatant	37.3 1.2	0.578 7.300	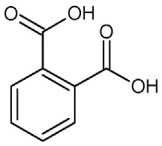

Table 2 (*continued*)

m/z	Metabolite	Chemical composition	Sample	Error (ppm)	Retention time (min)	Structure
149.0239 [M+H]	Phthalic anhydride	$C_8H_4O_3$	Supernatant	−9.4	2.91	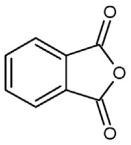
109.0086 [M-H]	Dihydroxy-benzene (catechol)	$C_6H_6O_6$	Supernatant	19.7	0.47	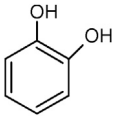

Catechol was also identified in supernatants of *C. tropicalis* (Kashyap et al., 2020) and catechol conjugates as by-products of lindane degradation by *Rhodotorula* sp. (Salam et al., 2013).

Metabolic profiling studies to elucidate yeast degradation of PAHs are scarce (Hadibarata et al., 2017; Kamyabi et al., 2018; Kashyap et al., 2020), indicating that further efforts are needed in this field to fully understand the process and device future applications.

3.5. Transcriptome pre-processing, assembly and analysis

The assembled transcriptome of *R. mucilaginosa* EXF-1630 contained 19,933 predicted genes and 23,815 transcripts with an average length of 1,526 nucleotides (Supplementary Material Table 1). This was twice the number of expected genes for this species, although typically assembled transcriptomes contain more genes than those identified in genomic sequences. The completeness assessment with BUSCO showed that 89% of the single-copy orthologues in Basidiomycota were present in the assembly, and from these 58% were in single-copy, 29% were artefactually duplicated and only 2% were fragmented (Fig. 4A). This indicated that the duplication level in the transcriptome is approximately 30%. Taking into consideration that the median length of transcripts (816 nt) was well below the average length, the duplication of the number of genes reflects an increase in very short sequences with no predicted function. The analysis of the coding potential of the assembly showed that approximately 74% of transcripts contained putative Open Reading Frames (ORFs). From the total predicted ORFs, 46% were complete (i.e. contained the starting Met codon and a STOP codon in the frame), 24% only contained the starting Met codon (5′ partial), 13% contained only a STOP codon (3' partial), and 18% contained a frame with coding potential but no starting Met or STOP codon (incomplete) (Fig. 4B). These metrics reveal sufficient quality of the transcriptome assembly, needed for subsequent differential analysis.

The clustering of transcriptome quantification profiles showed grouping of samples according to the experimental conditions (Fig. 4C and E). Furthermore, the heatmap of the quantification profiles showed a high abundance of low-count transcripts that could potentially reduce the statistical power of differential expression detection. Different cut-off filters based on a threshold CPM (counts per million) value were tested to remove noise from the data while keeping most transcripts (Fig. 4D). The result of transcripts filtering with CPM<0.05 in more than three samples is shown in Fig. 4E.

The count data were normalized prior to differential expression analysis using the RUVseq method, which resulted in all samples having a homogeneous distribution of relative log expression values (RLE) centered around 0, as expected (Fig. 4F). This metric can help to identify skewed count distributions that would bias differential expression inference. The principal component analysis of the normalized count data showed that samples from different experimental conditions were grouped in different areas of the PC1-PC2 principal component plot (Fig. 4G). Therefore, the PCA plot showed that the overall expression profile represented the biological conditions in which *R. mucilaginosa* was growing. This analysis also revealed that intersample variation in the PAH group was larger than in the glucose group, but this should not bias differential expression, since group samples are clustered in separate areas (Fig. 4G).

Finally, the differential expression analysis at transcript level showed that 870 transcripts were upregulated in *R. mucilaginosa* EXF-1630 when growing in PAHs as sole carbon source ($logFC_{PAHs\ vs\ glucose} > 2$, FDR<0.05), while 2,288 transcripts were downregulated in comparison to the control group growing in glucose ($logFC_{PAHs\ vs\ glucose} < -2$, FDR<0.05). The MA plot of the differential expression analysis (Fig. 4G) showed the distribution of statistically significant values of logFC across different expression ranges (represented as the mean of normalized counts). As shown in this plot, there is a high number of genes lowly expressed in the transcriptomes of *R. mucilaginosa* when growing in glucose media, but not expressed in media containing PAHs. Many of the transcripts could be the result of basal expression at permissive conditions, and therefore, not relevant for the biological comparison of these two metabolic states.

3.6. Multiomics integrated analysis focused on phenanthrene and benzo[a]pyrene degradation by Rhodotorula mucilaginosa EXF-1630

The analysis of the transcriptome of *R. mucilaginosa* EXF-1630 was focused on PAH biodegradation. All the assembled transcripts were mapped on the KEGG modules related to the metabolism of xenobiotic by CYP450 (M00980) and PAH degradation (M00624), which include the KEGG microbial pathways for Phe and BaP degradation.

A limited number of EXF-1630′s transcripts were annotated on the KEGG module M00980 (Supplementary Material Fig. S3). Transcripts encode glutathione-S-transferase (GST), CYP450 family 1 subfamily A (CYP1A1), CYP450 family 1 subfamily B (CYP1B1), and microsomal epoxide hydrolase (EPHX1), were mapped on the BaP degradation pathway included in KEGG M00980 (Supplementary Material Fig. S3). However, only *gst* genes were found differentially expressed in the transcriptome of *R. mucilaginosa* EXF-1630 exposed to PAHs at hypersaline conditions (Supplementary Material Table S2). 9-Hydroxy-benzo[α]pyrene (9-OH-B[a]P) was identified during the metabolic profile analysis (Table 2), suggesting that CYP450 could be involved in BaP degradation by EXF-1630. Between the by-products of the KEGG module M00980, only the 9-OH-B[a]P was detected as an

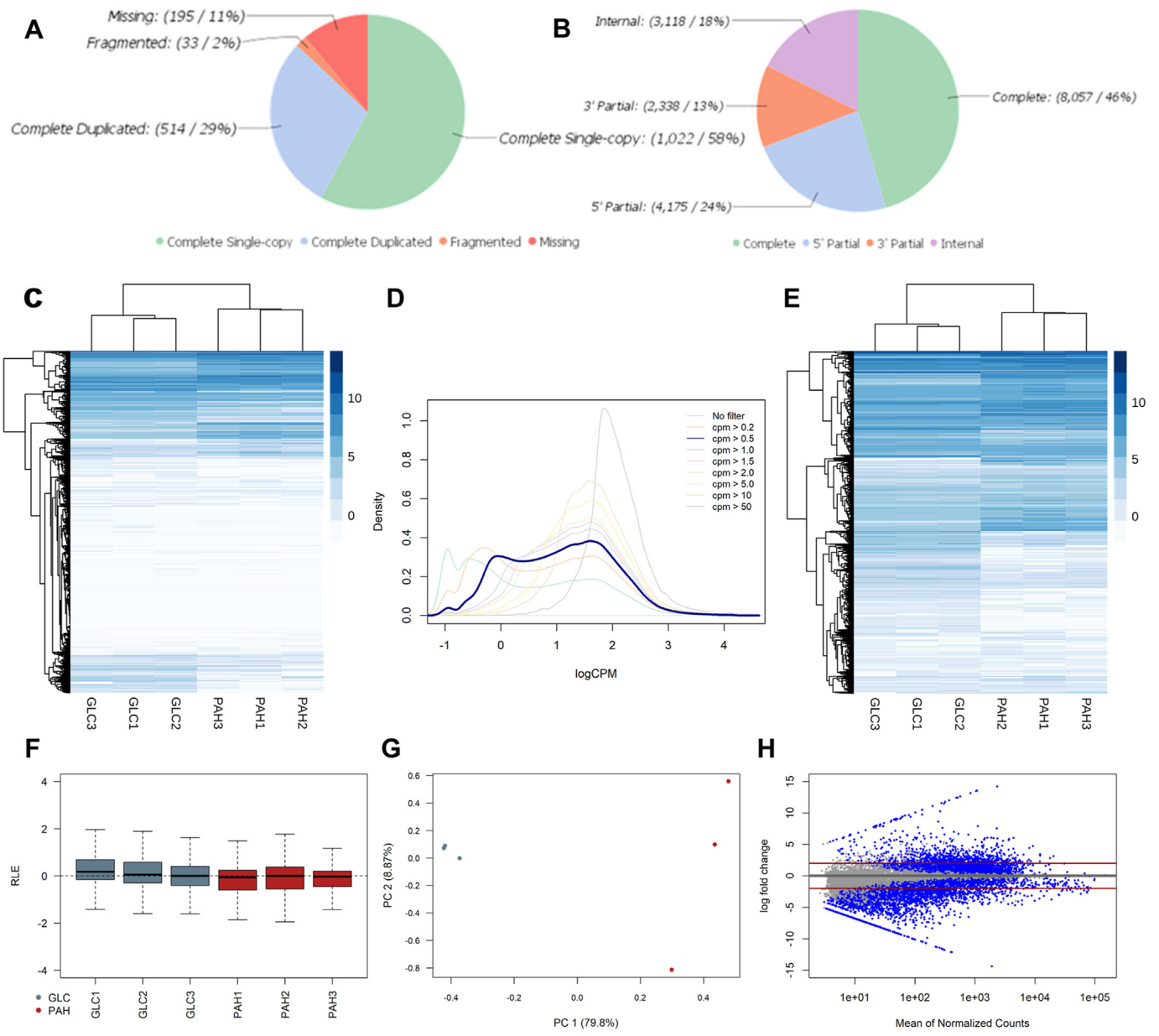

Fig. 4. Assembly, preprocessing, and differential expression analysis of *Rhodotorula mucilaginosa* EXF-1630 transcriptomes on PAH and glucose at hypersaline conditions (1 M NaCl). A) Assembly completeness assessed by BUSCO. B) Transcript coding potential assessed by CPAT. C) Transcriptome profiles before low-count read filtering. D) Evaluation of filtering cut-off based on the density distribution of read count level after filtering (see Materials and Methods section for filtering details), the selected cut-off is highlighted as a bold blue line. E) Transcriptome profiles after low-count read filtering using the selected filtering cut-off. F) Relative logarithmic expression (RLE) of transcriptome samples after RUVseq normalization procedure. G) Principal component analysis of transcriptome samples after RUVseq normalization procedure. H) MA-plot of differential expression of PAH transcriptome *versus* glucose transcriptome highlighting transcripts with FDR<0.05 in blue. Horizontal red lines mark the selected logFC cut-off value of (2,-2) to consider differentially expressed transcripts. (For interpretation of the references to color in this figure legend, the reader is referred to the Web version of this article.)

intermediary metabolite (Table 2 and Supplementary Material Fig. S3). The BaP derived, oxides, and diols, were not detected probably because they are metabolized rapidly due to their high cytotoxicity (Souza et al., 2016). Despite *gst* genes were upregulated (Supplementary Material Table S3), glutathionyl-BaP was also not detected (Supplementary Material Fig. S3), maybe because glutathionylated PAHs are quickly pumped into vacuoles (Morel et al., 2013). Glutathione plays a critical role in PAHs biodegradation due to the partially oxidized PAHs combined with glutathione, which show a reduction of toxicity, increase its water solubilization (important in intracellular trafficking and storage of toxic compounds), and activate subsequent metabolic steps for PAHs mineralization (Verdin et al., 2005; Morel et al., 2013).

Regarding the transcriptome analysis on the module M00624, no genes of EXF-1630 were annotated on this KEGG module (Supplementary Material Fig. S4). Interestingly, although different intermediary metabolites of the KEGG Phe degradation pathway included in M00624 were identified in this study (Table 2, Supplementary Material Fig. S4), any assembled transcript was annotated as one of the genes required to catalyze the production of these intermediary metabolites (Supplementary Material Fig. S4). For example, phenanthrene trans 9,10-dihydrodiol, 9-phenanthrol, hydroxy-naphtoic acid, and phthalic acid were identified in the metabolic profile of *R. mucilaginosa* EXF-1630 grown on

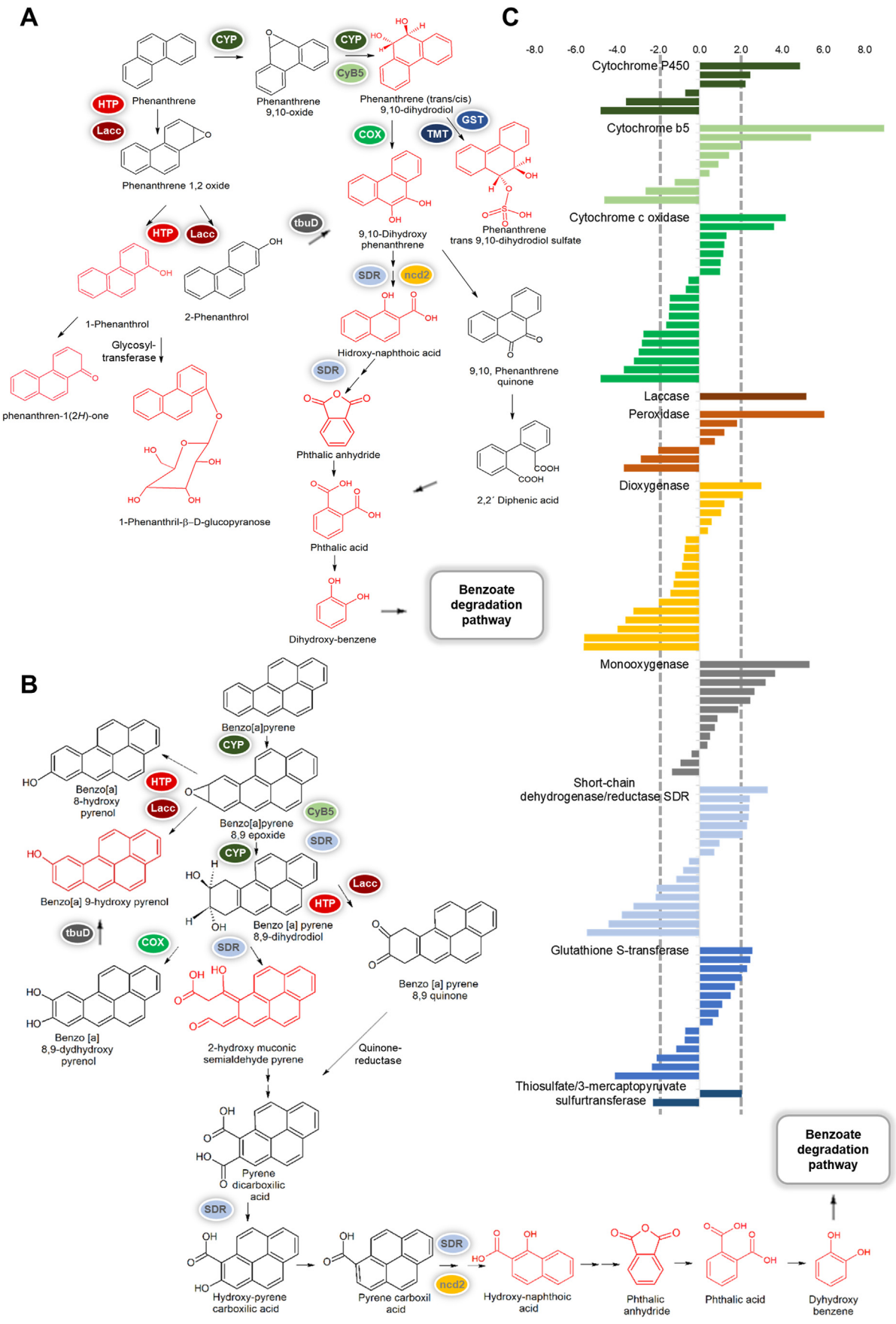
A
Phenanthrene
Phenanthrene 1,2 oxide
Phenanthrene 9,10-oxide
Phenanthrene (trans/cis) 9,10-dihydrodiol
9,10-Dihydroxy phenanthrene
Phenanthrene trans 9,10-dihydrodiol sulfate
2-Phenanthrol
1-Phenanthrol
phenanthren-1(2H)-one
1-Phenanthril-β-D-glucopyranose
Hidroxy-naphthoic acid
9,10, Phenanthrene quinone
2,2´ Diphenic acid
Phthalic anhydride
Phthalic acid
Dihydroxy-benzene
Benzoate degradation pathway
B
Benzo[a]pyrene
Benzo[a] 8-hydroxy pyrenol
Benzo[a]pyrene 8,9 epoxide
Benzo[a] 9-hydroxy pyrenol
Benzo [a] pyrene 8,9-dihydrodiol
Benzo [a] pyrene 8,9 quinone
Benzo [a] 8,9-dydhydroxy pyrenol
2-hydroxy muconic semialdehyde pyrene
Quinone-reductase
Pyrene dicarboxilic acid
Hydroxy-pyrene carboxilic acid
Pyrene carboxil acid
Hydroxy-naphthoic acid
Phthalic anhydride
Phthalic acid
Dyhydroxy benzene
Benzoate degradation pathway
C
-8.0 -6.0 -4.0 -2.0 0.0 2.0 4.0 6.0 8.0 10.0
Cytochrome P450
Cytochrome b5
Cytochrome c oxidase
Laccase
Peroxidase
Dioxygenase
Monooxygenase
Short-chain dehydrogenase/reductase SDR
Glutathione S-transferase
Thiosulfate/3-mercaptopyruvate sulfurtransferase

Table 3
Upregulated transcript possibly related to xenobiotic degradation according to KEGG database annotation.

Enzyme [EC]	KEGG reaction	Transcript	logFC	FDR
Benzoate degradation [map00362] **Benzoate 4- monooxygenase [1.14.14.92]**	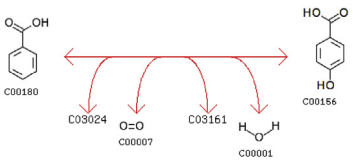	tr8775_c0_g1_i1	4.86	3.89e-31
Glutaryl-CoA dehydrogenase [1.3.8.6]		tr5831_c1_g3_i1	4.57	6.37e-58
3-Hydroxybutyryl-CoA dehydrogenase [1.1.1.157]	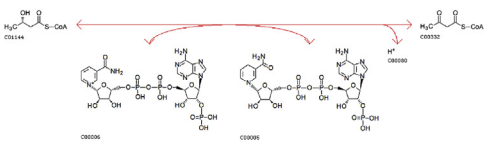	tr1018_c1_g1_i1	3.17	2.04e-13
Metabolism of xenobiotics by cytochrome P450 [map00980] **Glutathione S-transferase [2.5.1.18]**	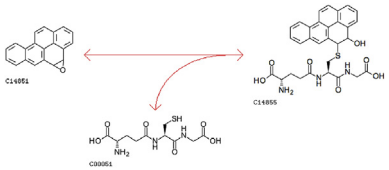	tr4532_c1_g1_i1	2.05	4.30e-12
Degradation of aromatic compounds [map01220] **Alcohol dehydrogenase (NADP+) [1.1.1.2]**	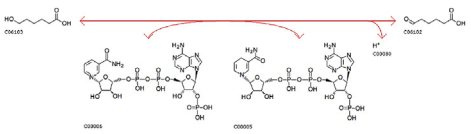	tr5933_c0_g2_i2	3.28	1.21e-11
Chloroalkane and chloroalkene degradation [map00625] **Aldehyde dehydrogenase (NAD+) [1.2.1.3]**	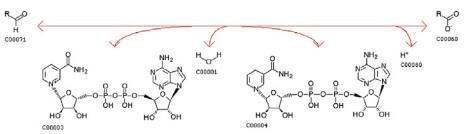	tr8571_c1_g1_i1	6.03	6.87e-59
Butanoate metabolism [map00650] - Caprolactam degradation [map00930] **3-Hydroxyacyl-CoA dehydrogenase [1.1.1.35]**	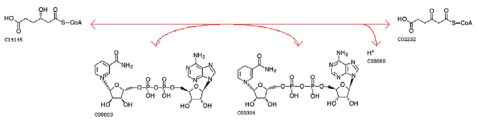	tr6237_c5_g2_i7	2.68	1.38e-06

logFC: the logarithm (to basis 2) of the fold change from treatment condition (polycyclic aromatic hydrocarbons) to control condition (glucose), FDR: *p* value adjusted for multiple testing with the Benjamini-Hochberg procedure which controls False Discovery Rate.

Phe and BaP (100 ppm as final concentration) at 1 M NaCl. The fact that any transcript was annotated on the KEGG module M00624, with some by-products being identified in this work (Supplementary Material Fig. S4), strongly suggests that new metabolic pathways involved in Phe degradation can occur in *R. mucilaginosa* EXF-1630. This reflects that more attention is needed to fully elucidate the microbial pathways for PAH degradation.

Based on the previous results and the obtained metabolic profile, we proposed the alternative pathways for Phe and BaP degradation by *R. mucilaginosa* EXF-1630 (Fig. 5A and B). These catabolic pathways show that Phe and BaP degradation by EXF-1630 could be plugged into the benzoate degradation pathway due to the identification of catechol as a by-product (Table 2, Fig. 5A and B). The transcriptomic results were integrated into these catabolic pathways. The genes encoding for the enzymes that catalyze the formation of the metabolites found in this study were thus identified in the transcriptome of *R. mucilaginosa* EXF-1630 (Fig. 5C).

1-Phenanthril β−D-glucopyranose and dihydroxybenzene (or

Fig. 5. Proposed degradation pathways of phenanthrene (Phe) (A) and benzo[a]pyrene (BaP) (B) by *Rhodotorula mucilaginosa* EXF-1630 at hypersaline conditions (1 M NaCl) based on transcriptomics and metabolic profiling results. Compounds in red were identified by UHPLC-MS in the supernatant and/or cells of *Rhodotorula mucilaginosa* EXF-1630 cultures. Possible enzymes involved in the biotransformation of intermediates were identified from the differentially expressed transcripts. C) Logarithmic fold change (logFC) of transcripts annotated to functions possibly involved in the biotransformation of Phe and BaP. Vertical dashed lines represent the (2,-2) logFC cut-off region. (For interpretation of the references to color in this figure legend, the reader is referred to the Web version of this article.)

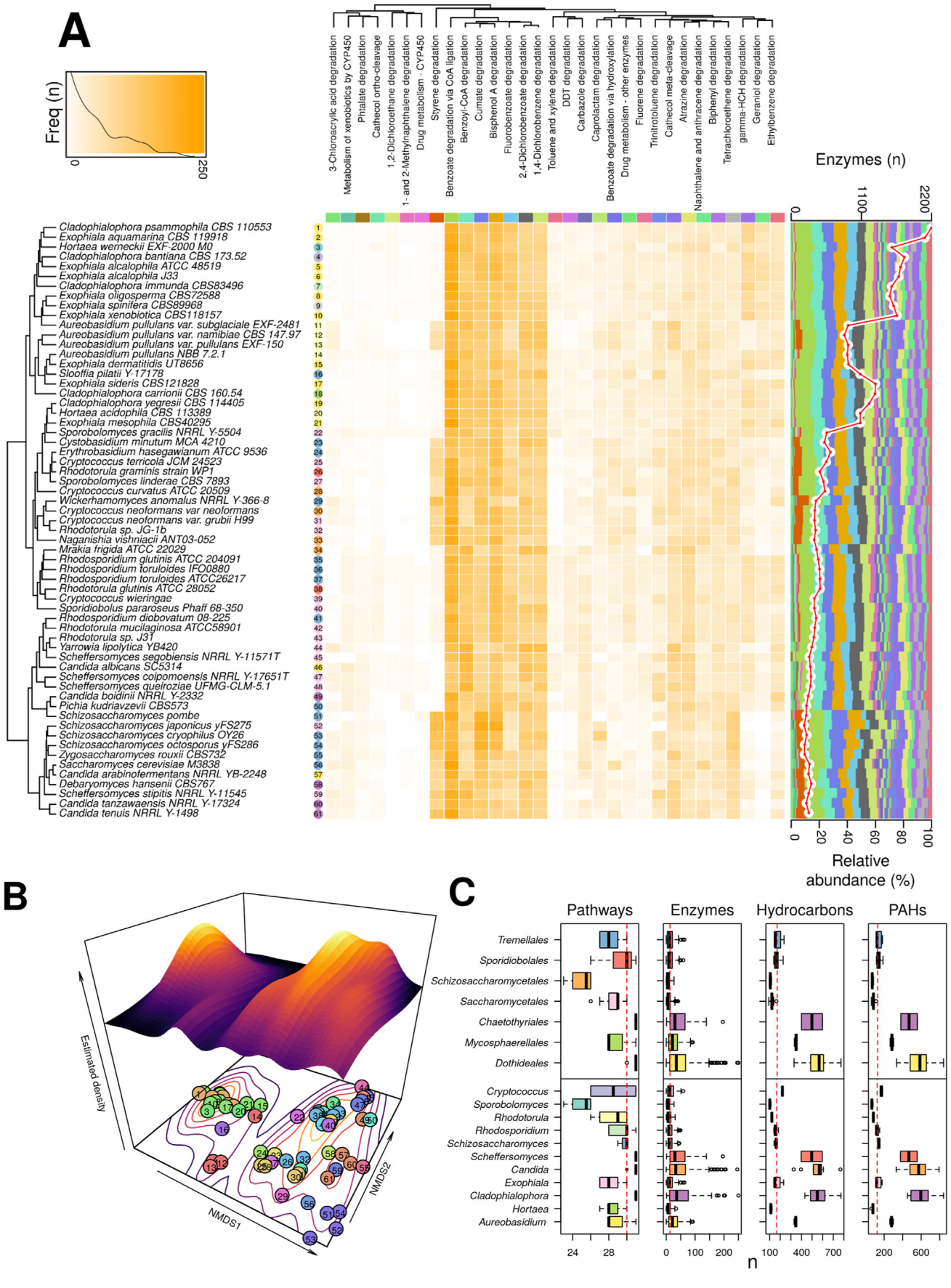
A
Freq (n)
0
250
3-Chloroacrylic acid degradation
Metabolism of xenobiotics by CYP450
Phtalate degradation
Cathecol ortho-cleavage
1,2-Dichloroethane degradation
1- and 2-Methylnaphthalene degradation
Drug metabolism - CYP450
Styrene degradation
Benzoate degradation via CoA ligation
Benzoyl-CoA degradation
Cumate degradation
Bisphenol A degradation
Fluorobenzoate degradation
2,4-Dichlorobenzoate degradation
1,4-Dichlorobenzene degradation
Toluene and xylene degradation
DDT degradation
Carbazole degradation
Caprolactam degradation
Benzoate degradation via hydroxylation
Drug metabolism - other enzymes
Fluorene degradation
Trinitrotoluene degradation
Cathecol meta-cleavage
Atrazine degradation
Naphthalene and anthracene degradation
Biphenyl degradation
Tetrachloroethene degradation
gamma-HCH degradation
Geraniol degradation
Ethylbenzene degradation
Enzymes (n)
0
1100
2200
Cladophialophora psammophila CBS 110553
Exophiala aquamarina CBS 119918
Hortaea werneckii EXF-2000 M0
Cladophialophora bantiana CBS 173.52
Exophiala alcalophila ATCC 48519
Exophiala alcalophila J33
Cladophialophora immunda CBS83496
Exophiala oligosperma CBS72588
Exophiala spinifera CBS89968
Exophiala xenobiotica CBS118157
Aureobasidium pullulans var. subglaciale EXF-2481
Aureobasidium pullulans var. namibiae CBS 147.97
Aureobasidium pullulans var. pullulans EXF-150
Aureobasidium pullulans NBB 7.2.1
Exophiala dermatitidis UT8656
Sloofia pilatii Y-17178
Exophiala sideris CBS121828
Cladophialophora carrionii CBS 160.54
Cladophialophora yegresii CBS 114405
Hortaea acidophila CBS 113389
Exophiala mesophila CBS40295
Sporobolomyces gracilis NRRL Y-5504
Cystobasidium minutum MCA 4210
Erythrobasidium hasegawianum ATCC 9536
Cryptococcus terricola JCM 24523
Rhodotorula graminis strain WP1
Sporobolomyces linderae CBS 7893
Cryptococcus curvatus ATCC 20509
Wickerhamomyces anomalus NRRL Y-366-8
Cryptococcus neoformans var neoformans
Cryptococcus neoformans var. grubii H99
Rhodotorula sp. JG-1b
Naganishia vishniacii ANT03-052
Mrakia frigida ATCC 22029
Rhodosporidium glutinis ATCC 204091
Rhodosporidium toruloides IFO0880
Rhodosporidium toruloides ATCC26217
Rhodotorula glutinis ATCC 28052
Cryptococcus wieringae
Sporidiobolus pararoseus Phaff 68-350
Rhodosporidium diobovatum 08-225
Rhodotorula mucilaginosa ATCC58901
Rhodotorula sp. J37
Yarrowia lipolytica YB420
Scheffersomyces segobiensis NRRL Y-11571T
Candida albicans SC5314
Scheffersomyces coipomoensis NRRL Y-17651T
Scheffersomyces queiroziae UFMG-CLM-5.1
Candida boidinii NRRL Y-2332
Pichia kudriavzevii CBS573
Schizosaccharomyces pombe
Schizosaccharomyces japonicus yFS275
Schizosaccharomyces cryophilus OY26
Schizosaccharomyces octosporus yFS286
Zygosaccharomyces rouxii CBS732
Saccharomyces cerevisiae M3838
Candida arabinofermentans NRRL YB-2248
Debaryomyces hansenii CBS767
Scheffersomyces stipitis NRRL Y-11545
Candida tanzawaensis NRRL Y-17324
Candida tenuis NRRL Y-1498
0
20
40
60
80
100
Relative abundance (%)
B
Estimated density
NMDS1
NMDS2
C
Pathways
Enzymes
Hydrocarbons
PAHs
Tremellales
Sporidiobolales
Schizosaccharomycetales
Saccharomycetales
Chaetothyriales
Mycosphaerellales
Dothideales
Cryptococcus
Sporobolomyces
Rhodotorula
Rhodosporidium
Schizosaccharomyces
Scheffersomyces
Candida
Exophiala
Cladophialophora
Hortaea
Aureobasidium
24
28
0
100
200
100
400
700
200
600
n

catechol) indicated the presence of two different metabolic pathways for phenanthrene (Fig. 5A), which were initiated by the K-region oxidation reactions in different positions. Oxidation at 1,2 carbon seems to be initiated by laccases (Lacc) and peroxidases (HTP) leading to the formation of phenanthrene 1–2 oxide, enzymes overexpressed under these conditions (4–8 LogFC respectively) following the formation of the relative phenanthrol. Oxidation to phenanthrene-1(2H)-one could occur spontaneously or mediated by oxidases that could represent a dead-end product. The second K-region oxidative reaction was mediated by CYP leading to the formation of phenanthrene (trans/cis)9,10-dihydrodiol. This gen was also overexpressed (LogFC = 5). The participation of cytochrome *c* oxidases (COX) and glutathione-S-transferase (GST)/thiosulfate/3-mercaptopyruvate sulfotransferase (TMT) could justify the presence of 9,10-dihydroxyphenathrene and phenanthrene trans 9,10-dihydrodiolsulfate, despite that some of them were underexpressed. Hydroxy-naphthoic acid was formed through an extradiolic ring fission reaction of 9,10-dihydroxyphenanthrene resulting from the K-region oxidation of phenanthrene mediated by short-chain dehydrogenase/reductases (SDR) and dioxygenases (ncd2). This metabolite was further transformed into phthalic acid and dihydroxybenzene indicating the presence of the benzoate degradation pathway (Fig. 5A). In the degradation of pyrene (Fig. 5B), only 2-hydroxy muconic semialdehyde pyrene was identified by UHPL/QTOF-MS, as well as hydroxynaphtoic, phthalic anhydride, phthalic acid, and dihydroxybenzene, which was not possible to distinguish between Phe or BaP pathway with the technology used. In this case, according to the putative pathway of Phe, hydroxylated products are formed by substitution in C8 and C9, mediated by CYP, HTP, and Lacc leading to the ring fission (Fig. 5B). This pathway has been described in the bacterium *Acinetobacter* under stress conditions to form dihydroxybenzene or catechol, mediated by catechol 1,2 dioxygenases (Kotoky et al., 2017).

Transcripts encoding for CYP450, cytochromes *b*5 (CyB5), COX, Lacc, HTP, ncd2, monooxygenases (tbuD), SDR, TMT, and GST were found upregulated (Fig. 5C). All these genes have been related to PAHs degradation by fungi (Aranda, 2016; Hernández-López et al., 2016; Huarte-Bonnet et al., 2018; Loss et al., 2019; Park and Choi, 2020; Peidro-Guzmán et al., 2020). Some of these genes (e.g. *gst, cyp450,* dehydrogenase) were also upregulated in the black yeast *Cladophialophora immunda* grown on toluene as a carbon source (Blasi et al., 2017). The expression levels of GSTs were also upregulated when the proteomic of *R. mucilaginosa* was studied after growth in the presence of arsenic and cadmium (Ilyas et al., 2016) and copper (Irazusta et al., 2012). Also, GST and SDR were overexpressed during the stress response of *R. mucilaginosa* exposed to patuline mycotoxin (Zheng et al., 2017).

We found up- and down-regulated genes for the same enzymatic activity (Fig. 5C). Interesting, preferential expression of transcripts was observed also in the EXF-1630′s transcriptome obtained in the presence of PAHs. For example, five isoforms of the transcript tr5746 encoding for a CyB5 were found differentially expressed, with three of them upregulated and two downregulated (Supplementary Material Table S3). TMT showed a similar transcriptomic profile with differentially expressed isoforms of the transcript tr6422 (Supplementary Material Table S3). Similar observations were evidenced for several genes (Supplementary Material Table S3). Our results suggest that preferential expression of transcripts could be an important genetic mechanism during PAH degradation by *R. mucilaginosa* EXF-1630. This fact is reported for the first time in fungi exposed to polyaromatic hydrocarbons.

Although some *lacc* and *htp* genes were differentially expressed, no enzymatic activity for laccase and peroxidase was detected in the EXF-1630′ supernatants after growth with Phe and BaP. These extracellular enzymes have been recognized as pivotal proteins for PAHs biodepletion by fungi (Aranda, 2016) and have been found differentially expressed in other fungi exposed to polyaromatic hydrocarbons (Gao et al., 2019). The observed differences can be attributed to different techniques as well as to the stability of the enzymes.

Other genes related to xenobiotic degradation according to the KEGG modules were also upregulated (Table 3).

3.7. Genomic analysis of xenobiotics metabolism in yeasts

A surprising diversity of yeasts inhabit a wide range of environments, from soil in polluted environments, cold and hot deserts, to ice and water in glaciers, hypersaline lakes, and deep-sea (Péter et al., 2017). Yeasts are polyphyletic and characterized by high metabolic plasticity that sustains diverse physiological traits and heterotrophic lifestyles (Péter et al., 2017), as reflected also in the genomes (Peter et al., 2018; Shen et al., 2018). Although genomic mining enables unprecedented insights on genes related to the xenobiotic metabolism, to the best of our knowledge, no published work so far focused on this topic. To address this gap, we examined 31 xenobiotic degradation pathways in 61 yeast genomes publicly available (Fig. 6A–C) (Supplementary Material Table S1) in the MycoCosm database (https://mycocosm.jgi.doe.gov/mycocosm/home). A taxonomically diverse group of ascomycetous and basidiomycetous yeasts, some also recognized for xenobiotic biodegradation capabilities (e.g. *Aureobasidium, Candida, Cryptococcus, Exophiala, Rhodosporidium, Rhodotorula,* etc.) were included in this genomic analysis.

The genome-scaling inferences showed that the 61 selected yeast species could potentially degrade a heterogeneous group of structurally diverse environmental pollutants (Fig. 6A). The 31 analyzed xenobiotic metabolic pathways displayed a widespread distribution in different yeast lineages. The presence of these biodegradative pathways indicates that yeast genomes of selected yeasts are differently enriched in genes encoding enzymes related to degradation of xenobiotics, and the differences can be only partially explained by their genus. Enzymes for the degradation of benzoate, benzoyl-CoA, cumate, bisphenol A, fluorobenzoate, dichlorobenzoate, and dichlorobenzene are fairly common in all 61 yeasts (Fig. 6A). However, some metabolic traits as degradation of chloroacrylic acid, phthalate, catechol ortho-cleavage, dichloroethane, and methylnaphtalene are underrepresented. Interestingly, the xenobiotic and drug metabolism mediated by CYP450 showed a limited number of annotated genes. We hypothesize that CYP450, one of the most pivotal enzymes involved in detoxification processes in many filamentous fungi (Aranda, 2016), is not crucial in yeasts. Possibly, due to the presence of not yet characterized

Fig. 6. Genomic analysis of xenobiotics metabolism and biodegradation in yeasts. A) The heatmap shows the number of enzymes annotated to each metabolic pathway. Absolute abundance of enzymes per species is shown in the right box as a red line. Relative abundances of enzymes per pathways are shown for each species as stacked barplots. Categories were clustered using the Jaccard distance and the UPGMA method. B) Non-metrical multidimensional scaling (NMDS) analysis obtained from the number of enzymes annotated in each metabolic pathway. The contour plot and the surface response were calculated using the kernel density estimation. C) Boxplots show the number of metabolic pathways, the number of total enzymes, the number of enzymes involved in hydrocarbon biodegradation, and the number of enzymes involved in polycyclic aromatic hydrocarbon bioegradation annotated in different orders (top row) and genera (bottom row). The dotted red lines represent the median of the distribution of total enzymes per category. Figure was produced on R package. (For interpretation of the references to color in this figure legend, the reader is referred to the Web version of this article.)

cytochromes and/or alternative undescribed metabolic pathways.

Similar observations were found by Shen et al. (2018) who reported the reconstruction and diversity of 45 discrete metabolic traits in 332 yeast genomes. They suggested an evolutionary transition from the metabolically complex common ancestor of yeasts, via major genomic reductions that included some metabolic pathways, to the current yeast diversity (Shen et al., 2018). These genomic reductions did not result in loss of metabolic capacities (Dujon and Louis, 2017) displayed by filamentous fungi with considerably larger genomes (e.g. *Aspergillus, Neurospora, Trichoderma*) (Wisecaver et al., 2014; Shen et al., 2018). Fig. 6A shows potential genomic reductions of pathways responsible for xenobiotic degradation that possibly occurred in yeast.

Non-metrical multidimensional scaling analysis (NMDS) obtained from the number of enzymes annotated in each metabolic pathway displays that two clusters can be easily distinguished (Fig. 6B). The first cluster comprises black yeasts *Hortea werneckii*, *Cladophialophora* spp., *Exophiala* spp. and *Aureobasidium pullulans* NBB 7.2.1, as well as *Slooffia pilatii* (Microbotrymycetes) (Fig. 6B). Other *Aureobasidium* strains (e.g. *A. namibiae, A. pullulans,* and *A. subglaciale*), group separately, reflecting a different metabolic capacity to degrade xenobiotics. This first distribution was mainly formed by Ascomycota representatives (except *S. pilatii*, which is very relevant, it seems that the degradation skills of *S. pilatii* are more similar to these Ascomycota than to their Basidiomycota peers).

The second cluster identified by the NMDS analysis was more heterogeneous at the genus and metabolic levels. This one showed a density gradient with the yeast cluster in the higher density. *R. mucilaginosa* was placed in this cluster together with other members of the Sporidiobolaceae family (e.g. *Rhodosporidium glutinis, Rhodosporidium toruloides, Rhodosporidium diobovatum, Sporidiobolus pararoseus, Sporobolomyces gracilis*) (Fig. 6B) indicating that all these species share similar metabolic skills related to the removal of xenobiotics. Other basidiomycetous yeasts such as *Mrakia frigida* and *Naganishia vishniacii* were also grouped in this cluster.

Saccharomyces cerevisiae and some *Schizosaccharomyces* species (*S. octosporus, S. japonicus,* and *S. pombe*) were grouped in a more sparse region of the NMDS (Fig. 6B). This indicates a limited metabolic arsenal for the degradation of xenobiotic compounds; therefore, they were included in the analysis as negative controls. These yeasts showed a very low abundance (or complete lack) of genes for geraniol, ethylbenzene, and gamma-hexachlorocyclohexane (gamma-HCH) degradation.

Genomic analysis revealed the higher number of catabolic pathways and enzymes in the orders *Dothideales, Chaetothyriales, Mycosphaerellales,* and *Sporidiobolales* (Fig. 6C), recognized for their genomic potential to degrade hydrocarbons, and in particular PAHs. The same analysis at the genus level identified *Aureobasidium, Candida, Cladophialophora, Exophiala,* and *Scheffersomyces* as the most promising genera to degrade hydrocarbons and PAHs in particular (Fig. 6C). Except for *Scheffersomyces*, they were largely reported as hydrocarbon degraders (Dallinger et al., 2016; Blasi et al., 2017; Zajc et al., 2019; Ide-Pérez et al., 2020).

The present analysis highlights the great potential of taxonomically diverse yeast species as xenobiotic degraders. This is the first attempt to examine the genetic diversity of yeasts related to xenobiotic metabolism through a genome-scaling inference meta-analysis. Additional efforts will be needed to investigate in depth the genomic co-occurrence of the biodegradation pathways in yeasts.

4. Conclusions

Polyextremotolerant yeast *R. mucilaginosa* EXF-1630 is a promising agent for biodegradation of PAHs at hypersaline conditions. This strain utilizes Phe and BaP as sole carbon source with the same efficiency as glucose. Toxicological tests on a model bacterium, a plant, and two types of human cells resulted in no observed cytotoxic effects. This was the first analysis of metabolic and transcriptomic responses on PAH degradation in yeasts. Multiomic analyses brought to light that CYP450 monooxygenases and glycosyl-transferases, in combination with the phthalic acid pathway, are the main PAHs detoxification mechanisms. Genomic mining of taxonomically diverse publicly available yeast genomes showed that some yeasts could degrade a heterogeneous group of structurally diverse environmental pollutants, despite genome reductions. Therefore, yeasts -that so far have been poorly investigated- represent an interesting tool for the degradation of xenobiotics.

Author contributions

Ramón A. Batista-García, Conceptualization, Project administration, Funding acquisition, Supervision, Writing – original draft preparation. All the authors: Methodology, Data curation, Investigation, Writing-Reviewing, and Editing.

Declaration of competing interest

The authors declare that they have no known competing financial interests or personal relationships that could have appeared to influence the work reported in this paper.

Acknowledgments

The authors are grateful to Alfonso Leija, Arielle Ariste, Olivier Sabori, Verónica Lira, Angélica Ortega, Marcela Ayala, Nilda de C. Sánchez, Lyselle Ruiz, Gisell Valdés, Deborah González, Clementina Pozo, Irina Jiménez, Adriana Otero, Carlos Amero, Daniela Escamilla, and María del Rayo Sánchez-Carbente for their technical support. LMA, HPG, YPLl, TMP, and AFS thank the National Council for Science and Technology of Mexico (Conacyt) for the received scholarships. HPG and YPLl received a fellowship from the Emerging Leaders in the Americas Program.

Appendix A. Supplementary data

Supplementary data to this article can be found online at https://doi.org/10.1016/j.envpol.2020.116358.

Funding

This work was supported by Project Conacyt-CB-285816, Project Conacyt Vocaciones Científicas 1004, Project Conacyt-DADC-311684, and Project-SEP-PRODEP-UAEMOR-PITC-381.

References

Addis, M.F., Tanca, A., Landolfo, S., Abbondio, M., Cutzu, R., Biosa, G., Pagnozzi, D., Uzzau, S., Mannazzu, I., 2016. Proteomic analysis of *Rhodotorula mucilaginosa*: dealing with the issues of a non-conventional yeast. Yeast 33 (8), 433–449.

Alegbeleye, O.O., Opeolu, B.O., Jackson, V.A., 2017. Polycyclic aromatic hydrocarbons: a critical review of environmental occurrence and bioremediation. Environ. Manag. 60, 758–783.

Ali, I., Khaliq, S., Sajid, S., Akbar, A., 2019. Biotechnological applications of halophilic fungi: past, present, and future. In: Tiquia-Arashiro, S., Grube, M. (Eds.), Fungi in Extreme Environments: Ecological Role and Biotechnological Significance. Springer, Cham, pp. 291–306.

Aranda, E., Ullrich, R., Hofrichter, M., 2010. Conversion of polycyclic aromatic hydrocarbons, methyl naphthalenes and dibenzofuran by two fungal peroxygenases. Biodegradation 21 (2), 267–281.
Aranda, E., 2016. Promising approaches towards biotransformation of polycyclic aromatic hydrocarbons with Ascomycota fungi. Curr. Opin. Biotechnol. 38, 1–8.
Aranda, E., Godoy, P., Reina, R., Badia-Fabregat, M., Rosell, M., Marco-Urrea, E., García-Romera, I., 2017. Isolation of ascomycota fungi with capability to transform pahs: insights into the biodegradation mechanisms of *Penicillium oxalicum*. Int. Biodeterior. Biodegrad. 122, 141–150.
Bano, A., Hussain, J., Akbar, A., Mehmood, K., Anwar, M., Hasni, M.S., Ullah, S., Sajid, S., Ali, I., 2018. Biosorption of heavy metals by obligate halophilic fungi. Chemosphere 199, 218–222.
Belloch, C., Pelaez, A.I., Sánchez, J., Kurtzman, C.P., 2020. *Wickerhamiella verensis f.a.* sp. nov., a novel yeast species isolated from subsoil groundwater contaminated with hydrocarbons and from a human infection. Int. J. Syst. Evol. Microbiol. 70, 2420–2425.
Blasi, B., Tafer, H., Kustor, C., Poyntner, C., Ksenija-Lopandic, K., Sterflinger, K., 2017. Genomic and transcriptomic analysis of the toluene degrading black yeast *Cladophialophora immunda*. Sci. Rep. 7, 11436.
Bolger, A.M., Lohse, M., Usadel, B., 2014. Trimmomatic: a flexible trimmer for Illumina sequence data. Bioinformatics 30 (15), 2114–2120.
Bray, N.L., Pimentel, H., Melsted, P., Pachter, L., 2016. Near-optimal probabilistic RNA-seq quantification. Nat. Biotechnol. 34 (5), 525–527.
Camacho-Morales, R.L., García-Fontana, C., Fernández-Irigoyen, J., Santamaría, E., González-López, J., Manzanera, M., Aranda, E., 2018. Anthracene drives subcellular proteome-wide alterations in the degradative system of *Penicillium oxalicum*. Ecotoxicol. Environ. Saf. 159, 127–135.
Casillas, R.P., Crow, S.A., Heinze, T.M., Deck, J., Cerniglia, C.E., 1996. Initial oxidative and subsequent conjugative metabolites produced during the metabolism of phenanthrene by fungi. J. Ind. Microbiol. Biotechnol. 16 (4), 205–215.
Castresana, J., 2000. Selection of conserved blocks from multiple alignments for their use in phylogenetic analysis. Mol. Biol. Evol. 17 (4), 540–552.
Cerniglia, C.E., 1997. Fungal metabolism of polycyclic aromatic hydrocarbons: past, present and future applications in bioremediation. J. Ind. Microbiol. Biotechnol. 19 (5–6), 324–333.
Chandran, P., Das, N., 2012. Role of plasmid in diesel oil degradation by yeast species isolated from petroleum hydrocarbon-contaminated soil. Environ. Technol. 33 (6), 645–652.
Collins, T., Margesin, R., 2019. Psychrophilic lifestyles: mechanisms of adaptation and biotechnological tolos. Appl. Microbiol. Biotechnol. 103, 2857–2871.
Dacco, C., Girometta, C., Asemoloye, M.D., Carpani, G., Picco, A.M., Tosi, S., 2020. Key fungal degradation patterns, enzymes, and their applications for the removal of aliphatic hydrocarbons in polluted soils: a review. Int. Biodeterior. Biodegrad. 147, 104866.
Dallinger, A., Duldhardt, I., Kabisch, J., Schlüter, R., Schauer, F., 2016. Biotransformation of cyclohexane and related alicyclic hydrocarbons by Candida maltose and Trichosporon species. Int. Biodeterior. Biodegrad. 107, 132–139.
de Menezes, G.C.A., Amorim, S.S., Gonçalves, V.N., Godinho, V.M., Simões, J.C., Rosa, C.A., Rosa, L.H., 2019. Diversity, distribution, and ecology of fungi in the seasonal snow of Antarctica. Microorganisms 7, 445.
Deeba, F., Pruthi, V., Negi, Y.S., 2018. Aromatic hydrocarbon biodegradation activates neutral lipid biosynthesis in oleaginous yeast. Bioresour. Technol. 255, 273–280.
Deligios, M., Fraumene, C., Abbondio, M., Mannazzu, I., Tanca, A., Addis, M.F., Uzzau, S., 2015. Draft genome sequence of *Rhodotorula mucilaginosa*, an emergent opportunistic pathogen. Genome Announc. 3 (2), e00201–e00215.
Dujon, B.A., Louis, E.J., 2017. Genome diversity and evolution in the budding yeasts (*Saccharomycotina*). Genetics 206, 717–750.
Farag, S., Soliman, N.A., 2011. Biodegradation of crude petroleum oil and environmental pollutants by *Candida tropicaliss* strain. Braz. Arch. Biol. 54 (4), 821–830.
Fu, W., Xu, M., Sun, K., Hu, L., Cao, W., Dai, C., Jia, Y., 2018. Biodegradation of phenanthrene by endophytic fungus *Phomopsis liquidambari* in vitro and in vivo. Chemosphere 203, 160–169.
Gao, R., Hao, D.C., Hu, W., Song, S., Li, S.Y., Ge, G.B., 2019. Transcriptome profile of polycyclic aromatic hydrocarbon-degrading fungi isolated from taxus rhizosphere. Curr. Sci. 116, 1218–1228.
Garapati, V.K., Mishra, S., 2012. Hydrocarbon degradation using fungal isolate: nutrients optimized by combined grey relational analysis. Int. J. Eng. Res. Afr. 2, 390–399.
Girotti, S., Ferri, E.N., Fumo, M.G., Maiolini, E., 2007. Monitoring of environmental pollutants by bioluminescent bacteria. Anal. Chim. Acta 608, 2–29.
González-Abradelo, D., Pérez-Llano, Y., Peidro-Guzmán, H., del Rayo Sánchez-Carbente, M.d, Folch-Mallol, J.L., Aranda, E., Kumar - Vaidyanathan, V., Cabana, H., Gunde-Cimerman, N., Batista-García, R.A., 2019. First demonstration that ascomycetous halophilic fungi (*Aspergillus sydowii* and *Aspergillus destruens*) are useful in xenobiotic mycoremediation under high salinity conditions. Bioresour. Technol. 279, 287–296.
Grabherr, M.G., Haas, B.J., Yassour, M., Levin, J.Z., Thompson, D.A., Amit, I., Adiconis, X., Fan, L., Raychowdhury, R., Zeng, Q., Chen, Z., Mauceli, E., Hacohen, N., Gnirke, A., Rhind, N., di Palma, F., Birren, B.W., Nusbaum, C., Lindblad-Toh, K., Friedman, N., Regev, A., 2011. Full-length transcriptome assembly from RNA-seq data without a reference genome. Nat. Biotechnol. 29 (7), 644–652.
Guarino, C., Spada, V., Sciarrillo, R., 2017. Assessment of three approaches of bioremediation (natural attenuation, landfarming and bioagumentation – assistited landfarming) for a petroleum hydrocarbons contaminated soil. Chemosphere 170, 10–16.
Guisado, I.M., Purswani, J., González-López, J., Pozo, C., 2016. An extractive membrane biofilm reactor as alternative technology for the treatment of methyl tert-butyl ether contaminated water. Biotechnol. Prog. 32 (5), 1238–1245.
Gunde-Cimerman, N., Oren, A., Plemenitas, A., 2005. Adaptation to life at high salt concentrations in archaea, bacteria, and eukarya. Cellular origin. Life in extreme habitats and astrobiology. Springer Sci. Rev. 9.
Gupta, S., Pathak, B., Fulekar, M.H., 2015. Molecular approaches for biodegradation of polycyclic aromatic hydrocarbon compounds: a review. Rev. Environ. Sci. Biotechnol. 14, 241–269.
Hadibarata, T., Khudhair, A.B., Kristanti, R.A., Kamyab, H., 2017. Biodegradation of pyrene by *Candida* sp. S1 under high salinity conditions. Bioproc. Biosyst. Eng. 40, 1411–1418.
Haritash, A.K., Kaushik, C.P., 2009. Biodegradation aspects of polycyclic aromatic hydrocarbons (pahs): a review. J. Hazard Mater. 169, 1–15.
Harrison, F.C., 1928. A systematic study of some torulae. Third Series Trans. Roy. Soc. Can. 22, 187–225. Section V.
Hashem, M., Alamri, S.A., Al-Zomyh, S.S.A.A., Alrumman, S.A., 2018. Biodegradation and detoxification of aliphatic and aromatic hydrocarbons by new yeast strains. Ecotoxicol. Environ. Saf. 151, 28–34.
Hernández-López, E.L., Perezgasga, L., Huerta-Saquero, A., Mouriño-Pérez, R., Vazquez-Duhalt, R., 2016. Biotransformation of petroleum asphaltenes and high molecular weight polycyclic aromatic hydrocarbons by *Neosartorya fischeri*. Environ. Sci. Pollut. Res. 23, 10773–10784.
Hesham, A.E.L., Wang, Z., Zhang, Y., Zhang, J., V, W.L., Yang, M., 2006. Isolation and identification of a yeast strain capable of degrading four and five ring aromatic hydrocarbons. Ann. Microbiol. 56 (2), 109–112.
Hesham, A.E.L., Alamri, S.A., Khan, S., Mahmoud, M.E., Mahmoud, H.M., 2009. Isolation and molecular genetic characterization of a yeast strain able to degrade petroleum polycyclic aromatic hydrocarbons. Afr. J. Biotechnol. 8 (10), 2218–2223.
Hesham, A.E.L., Alrumman, S.A., ALQahtani, A.D.S., 2018. Degradation of toluene hydrocarbon by isolated yeast strains: molecular genetic approaches for identification and characterization[1]. Russ. J. Genet. 54 (8), 933–943.
Huarte-Bonnet, C., Kumar, S., Saparrat, M.C.N., Girotti1, J.R., Santana, M., Hallsworth, J.E., Pedrini, N., 2018. Insights into hydrocarbon assimilation by eurotialean and hypocrealean fungi: roles for CYP52 and CYP53 clans of cytochrome P450 genes. Appl. Biochem. Biotechnol. 184, 1047–1060.
Ide-Pérez, M.R., Fernández-López, M.G., Sánchez-Reyes, A., Leija, A., Batista-García, R.A., Folch-Mallol, J.L., Sánchez-Carbente, M.R., 2020. Aromatic hydrocarbon removal by novel extremotolerant *Exophiala* and *Rhodotorula* spp. from an oil polluted site in Mexico. J. Fungi. 6, 135.
Ilyas, S., Rehman, A., Coelho, A.V., Sheehan, D., 2016. Proteomic analysis of an environmental isolate of *Rhodotorula mucilaginosa* after arsenic and cadmium challenge: identification of a protein expression signature for heavy metal exposure. J. Proteom. 141, 47–56.
Irazusta, V., Estévez, C., Amoroso, M.J., Figueroa, L.I.C., 2012. Proteomic study of the yeast *Rhodotorula mucilaginosa* RCL-11 under copper stress. Biometals 25, 517–527.
Jarboui, R., Baati, H., Fetoui, F., Gargouri, A., Gharsallah, N., Ammar, E., 2012. Yeast performance in wastewater treatment: case study of *Rhodotorula mucilaginosa*. Environ. Technol. 33 (8), 951–960.
Jarros, I., Veiga, F., Corrêa, J., Barros, I., Gadelha, M., Voidaleski, M., Pieralisi, N., Pedroso, R., Vicente, V., Negri, M., Svidzinski, T., 2020. Microbiological and virulence aspects of *Rhodotorula mucilaginosa*. EXCLI J 19, 687–704.
Jiang, Y., Yang, K., Wang, H., Shang, Y., Yang, X., 2015. Characteristics of phenol degradation in saline conditions of a halophilic strain JS3 isolated from industrial activated sludge. Mar. Pollut. Bull. 99, 230–234.
Kamyabi, A., Nouri, H., Moghimi, H., 2018. Characterization of pyrene degradation and metabolite identification by *Basidioascus persicus* and mineralization enhancement with bacterial-yeast co-culture. Ecotoxicol. Environ. Saf. 163, 471–477.
Kanehisa, M., Sato, Y., 2020. KEGG Mapper for inferring cellular functions from protein sequences. Protein Sci. 29 (1), 28–35.
Kashyap, N., Roy, K., Moholkar, V.S., 2020. Mechanistic investigation in Co-biodegradation of phenanthrene and pyrene by *Candida tropicalis* MTCC 184. Int. J. Chem. Eng. 399, 125659.
Katoh, K., Standley, D.M., 2013. Mafft multiple sequence alignment software version 7: improvements in performance and usability. Mol. Biol. Evol. 30 (4), 772–780.
Kotoky, R., Das, S., Singha, L.P., Pandey, P., Singha, K.M., 2017. Biodegradation of Benzo (a) pyrene by biofilm forming and plant growth promoting *Acinetobacter* sp. strain PDB4. Environ. Technol. Inno. 8, 256–268.
Kumar, M.S., Nilanjana, D., 2017. Biodegradation of benzo (a) pyrene by *Rhodotorula* sp. NS01 strain isolated from contaminated soil sample. Res. J. Pharm. Technol. 10 (6), 1751–1757.
Lackey, C.A., Murthy, N., Press, O.W., Tirrell, D.A., Hoffman, A.S., Stayton, P.S., 1999. Hemolytic activity of pH-responsive polymer-streptavidin bioconjugates. Bioconjugate Chem. 10 (3), 401–405.
Leelaruji, W., Buathong, P., Kanngan, P., Piamtongkamb, R., Chulalaksananukul, S., Wattayakorn, G., Chulalaksananukul, W., 2013. Biodegradation of poly-aromatic hydrocarbons *Aureobasidium pullulans* var. melanogenum. In: Proceedings of the International Conference of Environmental Science and Technology. Nevsehir, Turkey, pp. 18–21.
Liu, B., Wang, C., Liu, D., He, N., Deng, X., 2017. Hg tolerance and biouptake of an

isolated pigmentation yeast *Rhodotorula mucilaginosa*. PloS One 12 (3), e0172984.
Loss, E.M.O., Lee, M.K., Wu, M.Y., Martien, J., Chen, W., Amador-Noguez, D., Jefcoate, C., Remucal, C., Jung, S., Ki, S.C., Yu, J.H., 2019. Cytochrome P450 monooxygenase-mediated metabolic utilization of benzo [a] pyrene by *Aspergillus* species. Mol. Biol. Phys. 10, 1–15.
Love, M.I., Huber, W., Anders, S., 2014. Moderated estimation of fold change and dispersion for RNA-seq data with DESeq2. Genome Biol. 15, 550.
Margesin, R., 2014. Bioremediation and biodegradation of hydrocarbons by cold-adapted yeasts. In: Buzzini, P., Margesin, R. (Eds.), Cold-adapted Yeasts. Springer-Verlag Berlin Heidelberg, pp. 465–480.
McGenity, T.J., 2016. Halophilic hydrocarbon degraders. In: Timmis, K.N. (Ed.), Handbook of Hydrocarbon and Lipid Microbiology. Springer-Verlag Berlin Heidelberg, pp. 1940–1951.
Medina-Andrés, R., Solano-Peralta, A., Saucedo-Vázquez, J.P., Napsucialy-Mendivil, S., Pimentel-Cabrera, J.A., Sosa-Torres, M.A., Dubrovsky, J.G., Lira-Ruan, V., 2015. The nitric oxide production in the moss *Physcomitrella patens* is mediated by nitrate reductase. PloS One 10 (3).
Mikolasch, A., Donath, M., Reinhard, A., Herzer, C., Zayadan, B., Urich, T., Schauer, F., 2019. Diversity and degradative capabilities of bacteria and fungi isolated from oil-contaminated and hydrocarbon-polluted soils in Kazakhstan. Appl. Microbiol. Biotechnol. 103, 7261–7274.
Morel, M., Meux, E., Mathieu, Y., Thuillier, A., Chibani, K., Harvengt, L., Jacquot, J.P., Gelhaye, E., 2013. Xenomic networks variability and adaptation traits in wood decaying fungi. J. Microb. Biotechnol. 6, 248–263.
Oksanen, J., Kindt, R., Legendre, P., Hará, B.O., Simpson, G.L., Solymos, P., Stevens, M.H.H., Wagner, H., 2007. Community ecology package. The vegan Packge 1, 1, 15.
Park, H., Min, B., Jang, Y., Kim, J., Lipzen, A., Sharma, A., Andreopoulos, B., Johnson, J., Riley, R., Spatafora, J.W., Henrissat, B., Kim, K.H., Grigoriev, I.V., Kim, J.J., Choi, I.G., 2019. Comprehensive genomic and transcriptomic analysis of polycyclic aromatic hydrocarbon degradation by a mycoremediation fungus, *Dentipellis* sp. KUC8613. Appl. Microbiol. Biotechnol. 103, 8145–8155.
Park, H., Choi, I.G., 2020. Genomic and transcriptomic perspectives on mycoremediation of polycyclic aromatic hydrocarbons. Appl. Microbiol. Biotechnol. 104, 6919–6928.
Patel, A., Sartaj, K.m., Arora, N., Pruthi, V., Pruthi, P.A., 2017. Biodegradation of phenol via meta cleavage pathway triggers *de novo* TAG biosynthesis pathway in oleaginous yeast. J. Hazard Mater. 340, 47–56.
Peidro-Guzmán, H., Pérez-Llano, Y., González-Abradelo, D., Fernández-López, M.G., Dávila-Ramos, S., Aranda, E., Hernandez, D.R.O., García, A.O., Lira - Ruan, V., Pliego, O.R., Santana, M.A., Schnabel, D., Jiménez-Gómez, I., Mouriño-Pérez, R.R., Aréchiga-Carvajal, E.T., del Rayo Sánchez-Carbente, M., Folch-Mallol, J.L., Sánches-Reyes, A., Vaidyanathan, V.K., Cabana, H., Gunde-Cimerman, N., Batista-García, R.A., 2020. Transcriptomic analysis of polyaromatic hydrocarbon degradation by the halophilic fungus *Aspergillus sydowii* at hypersaline conditions. Environ. Microbiol.
Péter, G., Takashima, M., Čadež, N., 2017. Yeast habitats: different but global. In: Buzzini, P., Lachance, M.A., Yurkov, A. (Eds.), Yeasts in Natural Ecosystems: Ecology. Springer, Cham, pp. 39–71.
Peter, J., De Chiara, M., Friedrich, A., Yue, J.X., Pflieger, D., Bergström, A., Sigwalt, A., Barre, B., Freel, K., Llored, A., Cruaud, C., Labadie, K., Aury, J.M., Istace, B., Lebrigand, K., Barbry, P., Engelen, S., Lemainque, A., Wincker, P., Liti, G., Schacherer, J., 2018. Genome evolution across 1,011 *Saccharomyces cerevisiae* isolates. Nature 556, 339–344.
Prenafeta-Boldú, F.X., de Hoog, G.S., Summerbell, R.C., 2019. Fungal communities in hydrocarbon degradation. In: McGenity, T. (Ed.), Microbial Communities Utilizing Hydrocarbons and Lipids: Members, Metagenomics and Ecophysiology. Handbook of Hydrocarbon and Lipid Microbiology. Springer, Cham, pp. 307–342.
Price, M.N., Dehal, P.S., Arkin, A.P., 2010. FastTree 2 – approximately maximum-likelihood trees for large alignments. PloS One 5 (3).
Qureshi, A.A., Flood, K.W., Thompson, S.R., Janhurst, S.M., Inniss, C.S., Rokosh, D.A., 1982. Comparison of a luminescent bacterial test with other bioassays for determining toxicity of pure compounds and complex effluents. In: Pearson, J.G., Foster, R.B., Bishop, W.E. (Eds.), Aquatic Toxicology and Hazard Assessment in: Proceedings of the Fifth Conference. ASTM STP 766, pp. 179–195.
Rafiq, M., Hassan, N., Rehman, M., Hasan, F., 2019. Adaptation mechanisms and applications of psychrophilic fungi. In: Tiquia-Arashiro, S.M., Grube, M. (Eds.), Fungi in Extreme Environments: Ecological Role and Biotechnological Significance, pp. 157–174.
Ren, R., Sun, Y., Zhao, Y., Geiser, D., Ma, H., Zhou, X., 2016. Phylogenetic resolution of deep eukaryotic and fungal relationships using highly conserved low-copy nuclear genes. Genome Biol. Evol. 8 (9), 2683–2701.
Risso, D., Ngai, J., Speed, T.P., Dudoit, S., 2014. Normalization of RNA-seq data using factor analysis of control genes or samples. Nat. Biotechnol. 30 (9).
Salam, J.A., Lakshmi, V., Das, D., Das, N., 2013. Biodegradation of lindane using a novel yeast strain, *Rhodotorula* sp. VITJzN03 isolated from agricultural soil. World J. Microbiol. Biotechnol. 29, 475–487.
Seppey, M., Manni, M., Zdobnov, E.M., 2019. BUSCO: assessing genome assembly and annotation completeness. In: Kollmar, M. (Ed.), Gene Prediction. Methods. Mol. Biol., Humana, New York, NY, pp. 227–245, 1962.
Shen, X.X., Opulente, D.A., Kominek, J., Zhou, X., Steenwyk, J.L., Buh, K.V., Haase, M.A.B., Wisecaver, J.H., Wang, M., Doering, D.T., Boudouris, J.T., Schneider, R.M., Langdon, Q.K., Ohkuma, M., Endoh, R., Takashima, M., Manabe, R., Cadez, N., Libkind, D., Rosa, C.A., Virgilio, J.D., Hulfachor, A.B., Groenewald, M., Kurtzman, C.P., Hittinger, C.T., Rokas, A., 2018. Tempo and mode of genome evolution in the budding yeast subphylum. Cell 175, 1533–1545.
Shuryak, I., Tkavc, R., Matrosova, V.Y., Volpe, R.P., Grichenko, O., Klimenkova, P., Conze, I.H., Balygina, I.A., Gaidamakova, E.K., Daly, M.J., 2019. Chronic gamma radiation resistance in fungi correlates with resistance to chromium and elevated temperatures, but not with resistance to acute irradiation. Sci. Rep. 9, 11361.
Song, L., Florea, L., 2015. Rcorrector: efficient and accurate error correction for Illumina RNA-seq reads. GigaScience 4 (48).
Souza, T., Jennen, D., Delft, J., Herwijnen, M., Kyrtoupolos, S., Kleinjans, J., 2016. New insights into BaP-induced toxicity: role of major metabolites in transcriptomics and contribution to hepatocarcinogenesis. Arch. Toxicol. 90, 1449–1458.
Srivastava, S., Kumar, M., 2019. Biodegradation of polycyclic aromatic hydrocarbons (pahs): a sustainable approach. In: Shah, S., Venkatramanan, V., Prasad, R. (Eds.), Sustainable Green Technologies for Environmental Management. Springer, Singapore, pp. 111–139.
Tang, W., Wang, Y., Cai, Y., Liu, Sh, Zhang, J., He, Z., 2020. Genome sequence of a marine carotenoid producing yeast *Rhodotorula mucilaginosa* CYJ03. J. Ocean Univ. China 19, 466–472.
Tkavc, R., Matrosova, V.Y., Grichenko, O.E., Gostincar, C., Volpe, R.P., Klimenkova, P., Gaidamakova, E.K., Zhou, C.E., Stewart, B.J., Lyman, M.G., Malfatti, S.A., Rubinfeld, B., Courtot, M., Singh, J., Dalgard, C.L., Hamilton, T., Frey, K.G., Gunde-Cimerman, N., Dugan, L., Daly, M.J., 2018. Prospects for fungal bioremediation of acidic radioactive waste sites: characterization and genome sequence of *Rhodotorula taiwanensis* MD1149. Front. Microbiol. 8.
Uliasz, T.F., Hewett, S.J., 2000. A microtiter trypan blue absorbance assay for the quantitative determination of excitotoxic neuronal injury in cell culture. J. Neurosci. Methods 100, 157–163.
Varjani, S.J., 2017. Microbial degradation of petroleum hydrocarbons. Bioresour. Technol. 223, 277–286.
Verdin, A., Sahraoui, A.L.H., Newsam, R., Robinson, G., Durand, R., 2005. Polycyclic aromatic hydrocarbons storage by *Fusarium solani* in intracellular lipid vesicles. Environ. Pollut. 133, 283–291.
Wang, C., Wang, C.Y., Zhao, X.Q., Chen, R.F., Lan, P., Shen, R.F., 2013. Proteomic analysis of a high aluminum tolerant yeast *Rhodotorula taiwanensis* RS1 in response to aluminum stress. Biochim. Biophys. Acta 1834 (10), 1969–1975.
Wang, J.W., Luo, Z.H., Xu, W., Ding, J.F., Zheng, T.L., 2016. Transformation of dimethyl phthalate esters (DMPEs) by a marine red yeast *Rhodotorula mucilaginosa* isolated from deep sea sediments of the Atlantic Ocean. Int. Biodeterior. Biodegrad. 109, 223–228.
Wang, Q.M., Yurkov, A.M., Göker, M., Lumbsch, H.T., Leavitt, S.D., Groenewald, M., Theelen, B., Liu, X.Z., Boekhout, T., Bai, F.Y., 2016a. Phylogenetic classification of yeasts and related taxa within *Pucciniomycotina*. Stud. Mycol. 81, 149–189.
Wirth, I., Goldani, L., 2012. Epidemiology of Rhodotorula: an emerging pathogen. Inter. Persp. Infect. Dis. 465717.
Wisecaver, J.H., Slot, J.C., Rokas, A., 2014. The evolution of fungal metabolic pathways. PLoS Genet. 10 (12).
Wunder, T., Marr, J., Kremer, S., Sterner, O., Anke, H., 1997. 1-Methoxypyrene and 1,6-dimethoxypyrene: two novel metabolites in fungal metabolism of polycyclic aromatic hydrocarbons. Arch. Microbiol. 167, 310–316.
Yaguchi, A., Franaszek, N., O'Neill, K., Lee, S., Sitepu, I., Boundy-Mills, K., Blenner, M., 2020. Identification of oleaginous yeasts that metabolize aromatic compounds. J. Ind. Microbiol. Biotechnol. 389.
Zajc, J., Gostincar, C., Cernoša, A., Gunde-Cimerman, N., 2019. Stress-tolerant yeasts: opportunistic pathogenicity versus biocontrol potential. Genes 10 (42).
Zheng, X., Yang, Q., Zhao, L., Apaliya, M., Zhang, X., Zhang, H., 2017. Crosstalk between proteins expression and lysine acetylation in response to patulin stress in *Rhodotorula mucilaginosa*. Sci. Rep. 7, 13490.